

# The Dynamic Triple Gamma Prior as a Shrinkage Process Prior for Time-Varying Parameter Models

Peter Knaus and Sylvia Frühwirth-Schnatter  
Vienna University of Economics and Business

2023

## Abstract

Many current approaches to shrinkage within the time-varying parameter framework assume that each state is equipped with only one innovation variance for all time points. Sparsity is then induced by shrinking this variance towards zero. We argue that this is not sufficient if the states display large jumps or structural changes, something which is often the case in time series analysis. To remedy this, we propose the dynamic triple gamma prior, a stochastic process that has a well-known triple gamma marginal form, while still allowing for autocorrelation. Crucially, the triple gamma has many interesting limiting and special cases (including the horseshoe shrinkage prior) which can also be chosen as the marginal distribution. Not only is the marginal form well understood, we further derive many interesting properties of the dynamic triple gamma, which showcase its dynamic shrinkage characteristics. We develop an efficient Markov chain Monte Carlo algorithm to sample from the posterior and demonstrate the performance through sparse covariance modeling and forecasting of the returns of the components of the EURO STOXX 50 index.

## 1 Introduction

A standard time-varying parameter (TVP) model is a regression model with time-varying parameters:

$$y_t = \mathbf{x}_t \boldsymbol{\beta}_t + \varepsilon_t, \quad \varepsilon_t \sim \mathcal{N}(0, \sigma_t^2), \quad (1)$$

$$\boldsymbol{\beta}_t = \boldsymbol{\beta}_{t-1} + \mathbf{w}_t, \quad \mathbf{w}_t \sim \mathcal{N}_d(\mathbf{0}, \mathbf{Q}), \quad (2)$$

where the  $(1 \times d)$ -dimensional vector  $\mathbf{x}_t = (x_{1t} \ x_{2t} \ \cdots \ x_{dt})$  contains the regressors and  $y_t$  is the regressand, for  $t = 1, \dots, T$ . To simplify notation, we assume that  $x_{1t}$  corresponds to the intercept, i.e.  $x_{1t} = 1$ . If  $\mathbf{Q} = \text{Diag}(\theta_1, \dots, \theta_d)$ , then, for  $j = 1, \dots, d$ :

$$\beta_{jt} = \beta_{j,t-1} + w_{jt}, \quad w_{jt} \sim \mathcal{N}(0, \theta_j).$$

The system is initialized by assuming that the initial value  $\boldsymbol{\beta}_0$  is randomly drawn from the following normal distribution:  $\boldsymbol{\beta}_0 \sim \mathcal{N}_d(\boldsymbol{\beta}, \mathbf{Q})$ , where  $\boldsymbol{\beta} = (\beta_1, \dots, \beta_d)'$ . The error variance can either be assumed to be homoscedastic, meaning that  $\sigma_t^2 = \sigma^2$ , or follow the stochastic volatility specification of [Jacquier et al. \(1994\)](#), where the log volatility  $h_t = \log \sigma_t^2$  follows an AR(1) process:

$$h_t | h_{t-1}, \mu, \phi, \sigma_\eta^2 \sim \mathcal{N}(\mu + \phi(h_{t-1} - \mu), \sigma_\eta^2). \quad (3)$$

In this standard form, each state only has a single variance parameter (i.e.  $\theta_j$ ) for all  $T$  innovations. The underlying assumption is that there is a smoothness to the evolution of the states from one time

point to the next, as the light tails of the Gaussian distribution places little prior mass on innovations far from zero. Note here that smaller values of  $\theta_j$  imply smaller innovations on average, with the extreme case,  $\theta_j = 0$ , implying that  $\beta_{jt} = \beta_{j,t-1} = \beta_j$ . We refer to such models as time-varying parameter models with static shrinkage, or, equivalently, we use the slightly oxymoronic term “static time-varying parameter models”.

As these models are already quite flexible, proper regularization is important. In particular, it needs to be determined which regressors have an impact on the regressand and which of these impacts vary over time. Differentiating between these cases amounts to identifying which  $\beta_j$  and  $\theta_j$  are different from zero. While the former problem is one more closely related to variable selection, a task for which shrinkage priors were designed, the latter is one of *variance* selection. This was first recognized by [Frühwirth-Schnatter and Wagner \(2010\)](#), who managed to re-cast this issue into another variable selection problem through the introduction of the non-centered parameterization of the standard TVP model. In such a reparameterized state-space model, shrinkage priors can now also take on the challenge of variance selection, with little to no modification. This spawned a strand of the literature that investigated the performance of various shrinkage priors in this role, such as the Bayesian lasso prior ([Belmonte et al., 2014](#); [Park and Casella, 2008](#)), the normal-gamma prior ([Bitto and Frühwirth-Schnatter, 2019](#); [Griffin and Brown, 2017](#)), the Dirichlet-Laplace prior ([Huber et al., 2020](#); [Bhattacharya et al., 2015](#)) or the horseshoe prior ([Huber et al., 2020](#); [Carvalho et al., 2009](#)), to name a few. This is also the context in which the triple gamma prior was introduced and studied by [Cadonna et al. \(2020\)](#).

**Definition 1.1.** A random variable  $X$  has a triple gamma distribution with parameters  $a > 0$ ,  $c > 0$  and  $\kappa > 0$ , denoted by  $X \sim TG(a, c, \kappa)$ , if it has density

$$f(x; a, c, \kappa) = \frac{\Gamma(c + \frac{1}{2})}{\sqrt{2\pi\phi x} B(a, c)} U\left(c + \frac{1}{2}, \frac{3}{2} - a, \frac{\sqrt{x}}{2\phi}\right), \quad (4)$$

where  $\phi = \frac{2c}{\kappa a}$  and  $U(a, b, z)$  is the confluent hyper-geometric function of the second kind:

$$U(a, b, z) = \frac{1}{\Gamma(a)} \int_0^\infty e^{-zt} t^{a-1} (1+t)^{b-a-1} dt.$$

The triple gamma proved to have desirable shrinkage characteristics on its own, with a strong pole around the origin and heavy tails, while having the additional benefit of subsuming many other shrinkage prior choices. (Of the previously mentionend shrinkage priors, all but the Dirichlet-Laplace are special or limiting cases of the triple gamma.) The eponymous representation of the triple gamma is a compound distribution consisting of three gamma random variables, meaning that  $X|a, c, \kappa \sim TG(a, c, \kappa)$  is equivalent to

$$X|Y, \kappa \sim \mathcal{G}\left(\frac{1}{2}, \frac{\kappa}{2Y}\right), \quad Y|Z, a \sim \mathcal{G}\left(a, \frac{aZ}{2}\right), \quad Z|c \sim \mathcal{G}(c, c). \quad (5)$$

While a detailed discussion of the properties of the triple gamma is outside the scope of this paper, it is worth briefly mentioning the role the three hyperparameters  $a$ ,  $c$  and  $\kappa$  play.  $a$  acts as a pole parameter, with smaller values corresponding to more mass around the origin. This is important, as it helps to squash noise.  $c$  governs the behavior in the tails, with smaller values leading to heavier tails, allowing signals to filter through. Furthermore,  $c$  determines whether the prior moments exist, as the moments  $\mathbb{E}[X|a, c, \kappa]$

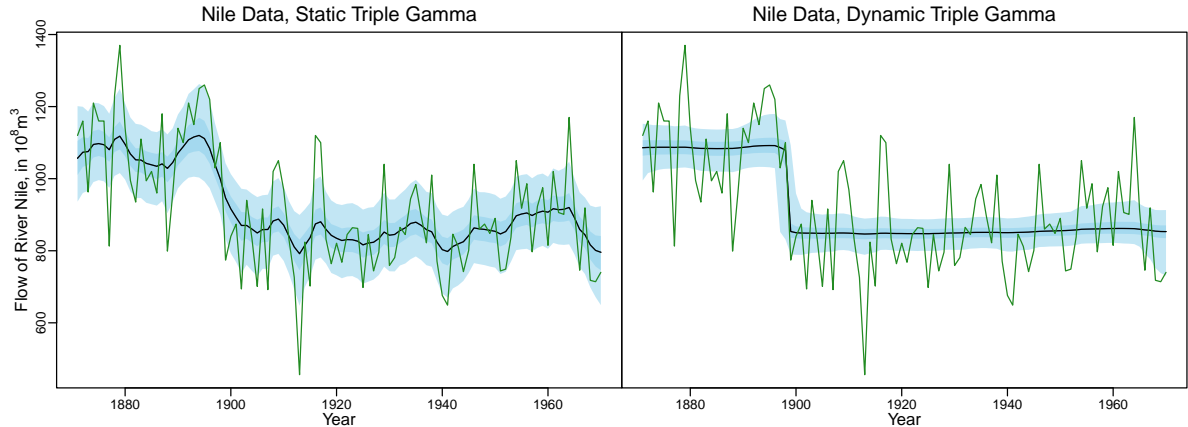


Figure 1: Posterior estimate of mean from local level model fit to Nile data set under static triple gamma and dynamic triple gamma (specifically with  $a = c = 0.5$ ). Black lines represents posterior medians, while shaded regions represent pointwise 50% and 95% credible intervals. The green line represents the observations.

exist up to  $k < 2c$ . Generally, the values of  $a$  and  $c$  should be chosen relatively close to zero, as this results in a prior with a pronounced pole at zero and heavy tails. Finally,  $\kappa$  acts as a global shrinkage parameter, with higher values leading to stronger shrinkage across the board. Readers interested in a more in-depth discussion are referred to [Cadonna et al. \(2020\)](#).

Despite their flexibility, static time-varying parameter models struggle when the assumption of constant variance of the innovations is not fulfilled. There are many underlying causes that could lead to such behavior, such as regime changes (e.g. changes in macroeconomic variables due to changes in government) or large, unexpected shocks (e.g. a sudden economic downturn or a pandemic), for example. In such cases, these models suffer from both over- and under-shrinkage of the innovations, as a single parameter governing the variance has to accommodate multiple different true underlying variances. As an illustrative example, consider the well-known Nile data set from [Cobb \(1978\)](#). It consists of 100 measurements of the annual flow of the river Nile at Aswan, with an apparent change-point near 1898, most likely due to a change in rainfall patterns ([Kraus, 1956](#)). Such a change-point problem is anathema to the static case, as it requires a limited number of large jumps (necessitating high variance in the innovations) followed and preceded by periods of low variance. The left-hand panel of [Figure 1](#) plots the posterior of the mean of a local level model<sup>1</sup> fit to this data set under a static triple gamma prior on both  $\beta$  and  $\theta$ . The aforementioned over-shrinkage is apparent around the change-point, as the shift downwards is quite gradual, where it should be fairly sharp. Under-shrinkage, on the other hand, can be seen to the left and right of the change-point, where it seems a lot of noise is tarnishing the estimate of the mean of the time series. Contrast this with the right-hand panel of [Figure 1](#), which graphs the mean of a local level model under the proposed dynamic triple gamma, which nicely picks up the change point while not suffering from the aforementioned under-shrinkage in the less volatile periods.

This deficiency of time-varying parameter models with static shrinkage has also been recognized by

<sup>1</sup>Estimation performed by the `shrinkTVP` ([Knaus et al., 2022](#)) package.

other authors, leading to a wealth of literature that aims to develop dynamic shrinkage, i.e. shrinkage priors that can adapt to locally differing levels of variance. An early discussion of dynamic linear models (of which time-varying parameter models are a special case) with time-varying variance can be found in [Petris et al. \(2009\)](#) and the accompanying R package `d1m` ([Petris, 2010](#)). Further pioneering work in this direction was undertaken by [Koop and Korobilis \(2012\)](#), who developed a time-varying Bayesian model averaging scheme and [Nakajima and West \(2013\)](#), who used a latent threshold approach to induce time-varying sparsity. Many other approaches are based on the idea of generalizing a shrinkage prior designed for variable selection to handle dynamic shrinkage. Due to its attractive theoretical properties and interpretability, the spike-and-slab approach ([Mitchell and Beauchamp, 1988](#); [George and McCulloch, 1993, 1997](#)) is a popular candidate for extension, with work in this direction done by [Huber et al. \(2019\)](#), [Uribe and Lopes \(2020\)](#), and [Ročková and McAlinn \(2021\)](#), among others. In contrast to this, a second strand of the literature is defined by a continuous shrinkage prior serving as the basis for generalization into a shrinkage process prior, with examples including work by [Kalli and Griffin \(2014\)](#), [Kowal et al. \(2019\)](#), [Irie \(2019\)](#) and [Huber and Pfarrhofer \(2021\)](#), among others. Finally, there exist modern approaches which are not as easily pigeonholed into these two categories, such as the mixture approach by [Hauzenberger et al. \(2021\)](#) or the tree-based contribution of [Hauzenberger et al. \(2022\)](#).

This paper seeks to contribute to the existing body of literature by introducing a stochastic process characterized by a marginal distribution that demonstrates favorable shrinkage properties and permits autocorrelation in the variances, all while remaining mathematically well understood. Specifically, the proposed process results in a marginal distribution that is triple gamma, while still allowing for autocorrelation in the variances of the innovations. The pronounced spike of the triple gamma marginal distribution encodes the prior information that most innovations will be fairly close to zero, while the heavy tails still allow for outliers. Accounting for autocorrelation, on the other hand, enables information on volatility of the variances to be shared across time points, something that could not be achieved by simply making the innovations i.i.d. triple gamma, for example.

As the triple gamma encompasses many popular shrinkage prior choices as special or limiting cases, this defines a whole class of stochastic processes with diverse shrinkage priors as marginal distributions. A notable aspect of our contribution lies in the ability of the process to feature a horseshoe marginal distribution that accommodates autocorrelation – a combination that, to the best of our knowledge, is novel within the existing literature. Despite these attractive features, the full conditional distributions of the posterior are mostly available in closed form, greatly simplifying estimation.

The rest of the paper is structured as follows - Section 2 introduces the dynamic triple gamma, discusses its properties, highlights its relationship to other approaches in the literature, and discusses hyperprior choices. Section 3 develops an efficient Markov chain Monte Carlo (MCMC) sampler to estimate TVP models under the dynamic triple gamma. Section 4 showcases the dynamic triple gamma by fitting a Cholesky SV-model to the returns of the components of the EURO STOXX 50 index and demonstrating the out-of-sample forecasting performance via log predictive density scores (LPDS). Finally, Section 5 concludes.

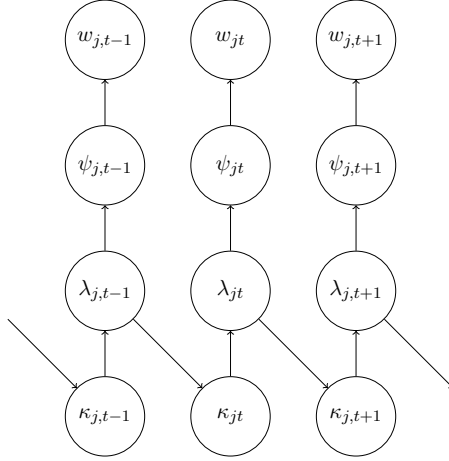


Figure 2: Interdependencies of the latent variables of the dynamic triple gamma prior represented as a directed graph.

## 2 The Dynamic Triple Gamma Prior

At a high level, loosening the assumption of non-time-varying variances amounts to adding a  $t$  subscript to the variance-covariance matrix  $\mathbf{Q}$  in the model introduced in Section 1:

$$y_t = \mathbf{x}_t \boldsymbol{\beta}_t + \varepsilon_t, \quad \varepsilon_t \sim \mathcal{N}(0, \sigma_t^2), \quad (6)$$

$$\boldsymbol{\beta}_t = \boldsymbol{\beta}_{t-1} + \mathbf{w}_t, \quad \mathbf{w}_t \sim \mathcal{N}_d(\mathbf{0}, \mathbf{Q}_t). \quad (7)$$

The difficulty lies in determining an appropriate stochastic process to govern  $\mathbf{Q}_t = \text{Diag}(\theta_1 \psi_{1t}, \dots, \theta_d \psi_{dt})$ . We begin by presenting the hierarchical representation of the proposed process, dubbed the dynamic triple gamma (DTG) prior, and will then delve into the detailed considerations that guided the specific distributional choices. Let  $w_{jt}$  denote the  $j^{\text{th}}$  element of the vector of innovations at time  $t$ , i.e.  $\mathbf{w}_t = (w_{1t}, \dots, w_{dt})'$ , as in (7). Then, a DTG process for  $\{w_{jt}^2\}_{t=1}^T$  is defined by the following hierarchical structure:

$$w_{jt} | \theta_j, \psi_{jt} \sim \mathcal{N}(0, \theta_j \psi_{jt}), \quad (8)$$

$$\psi_{jt} | \lambda_{jt}, c_j \sim \mathcal{G}^{-1}(c_j, \lambda_{jt}), \quad (9)$$

$$\lambda_{jt} | \kappa_{jt}, a_j, c_j, \rho_j \sim \mathcal{G}\left(a_j + \kappa_{jt}, \frac{a_j}{c_j} \frac{1}{1 - \rho_j}\right), \quad (10)$$

$$\kappa_{jt} | \lambda_{j,t-1}, a_j, c_j, \rho_j \sim \mathcal{P}\left(\frac{a_j}{c_j} \frac{\rho_j}{1 - \rho_j} \lambda_{j,t-1}\right). \quad (11)$$

To aid in the understanding of the interdependencies between the latent variables, a visualization of this structure as a directed graph can be found in Figure 2.

A few comments are in order. First, analogously to the inverse of  $\kappa$  in the static triple gamma shrinkage prior (see (4)),  $\theta_j$  governs the global shrinkage applied to the innovations of the state  $\beta_1, \dots, \beta_d$ . This can be seen by noting that  $\mathbb{V}[w_{jt} | \theta_j, \psi_{jt}] = \theta_j \psi_{jt}$  goes to zero as  $\theta_j$  goes to zero, or by examining (13), where the global shrinkage parameter of the marginal distribution ( $\kappa$  in (4)) depends inversely on

$\theta_j$ . Further, the proposed process nests the static shrinkage approach, as the two coincide when  $\psi_{jt} = 1$ . Second, following [Gourieroux and Jasiak \(2006\)](#), the choice of stochastic process governing  $\{\lambda_{jt}\}$  induces a marginal distribution that is well-known, namely  $\lambda_{jt}|a_j, c_j \sim \mathcal{G}\left(a_j, \frac{a_j}{c_j}\right)$ . Moreover, it leads to a process that is autocorrelated due to the dependence of  $\lambda_{jt}$  on  $\lambda_{j,t-1}$  through the contemporaneous value of  $\kappa_{jt}$ , with the strength of the autocorrelation governed by the parameter  $\rho_j$ . More precisely, this construction causes the expectation to be linearly dependent on the previous value in the series, meaning that  $\mathbb{E}[\lambda_{jt}|\lambda_{j,t-1}] = \rho_j \lambda_{j,t-1}$ . Note that, as  $\lambda_{jt}$  only has support on  $\mathbb{R}_+$ , this construction only allows for values of  $\rho_j$  in  $(0, 1)$ .

Finally, the choice of marginal distribution for  $\{\lambda_{jt}\}$  coupled with the distribution of  $\psi_{jt}|\lambda_{jt}, c_j$  leads to  $\psi_{jt}|a_j, c_j$  being marginally distributed as  $F(2a_j, 2c_j)$ . To see this, note that the F-distribution  $F(2a_j, 2c_j)$  has a representation as the ratio of two independent gamma distributions:

$$F(2a_j, 2c_j) \stackrel{d}{=} \frac{\mathcal{G}(a_j, 1)/a_j}{\mathcal{G}(c_j, 1)/c_j}.$$

This can be written as

$$F(2a_j, 2c_j) \stackrel{d}{=} \frac{\mathcal{G}(a_j, 1) c_j/a_j}{\mathcal{G}(c_j, 1)} \stackrel{d}{=} \mathcal{G}^{-1}(c_j, \mathcal{G}(a_j, a_j/c_j)),$$

which yields a novel representation of the triple gamma prior as gamma distribution mixed over an inverse gamma distribution (something which can also be useful during MCMC estimation, see [Section 3](#)):

$$\psi_{jt}|a_j, c_j \sim F(2a_j, 2c_j) \Leftrightarrow \psi_{jt}|\lambda_{jt}, c_j \sim \mathcal{G}^{-1}(c_j, \lambda_{jt}), \lambda_{jt}|a_j, c_j \sim \mathcal{G}\left(a_j, \frac{a_j}{c_j}\right). \quad (12)$$

Finally, using the fact that the triple gamma prior has a representation as a normal distribution mixed over an F distribution ([Cadonna et al., 2020](#)), it follows that

$$w_{jt}^2|\theta_j, a_j, c_j \sim TG(a_j, c_j, 2/\theta_j) \Leftrightarrow w_{jt}|\theta_j, \psi_{jt} \sim \mathcal{N}(0, \theta_j \psi_{jt}), \psi_{jt}|a_j, c_j \sim F(2a_j, 2c_j). \quad (13)$$

Therefore, the resulting process that governs the evolution of  $w_{jt}^2$  is marginally triple gamma, with the results from [Cadonna et al. \(2020\)](#) painting a rich picture of its shrinkage properties, while still allowing for dependence across time through the autoregressive parameter  $\rho_j$ .  $a_j$  and  $c_j$  have the same interpretation as in the static triple gamma case discussed in [Section 1](#), with  $a_j$  controlling the tail behavior and  $c_j$  controlling the tails. The prior information imbued in this construction builds on the argument in [Polson and Scott \(2011\)](#), in that a shrinkage prior should have substantial mass at zero (to squelch noise) combined with heavy tails (to let signals filter through), while expanding on it by allowing information to be shared across time points. The intuition behind how information is shared has overlap with the stochastic volatility in mean model of [Koopman and Hol Uspensky \(2002\)](#), meaning that a large variance at time  $t$  increases the probability of a large variance at time  $t + 1$ . A key difference, however, is that our marginal distribution additionally induces heavy shrinkage, encoding the prior information that one expects most innovations to be (very) close to zero.

As the horseshoe prior is a special case of the triple gamma prior, this also creates a blueprint for a stochastic process which is marginally horseshoe, while still allowing for autocorrelation. This sets it apart from other approaches, where the conditional distribution may be a horseshoe but the marginal is not well known.

## 2.1 Properties of the dynamic triple gamma

To gain further understanding of the dynamic triple gamma prior, one can rely on alternate representations of the process, which can be achieved by marginalizing out specific sets of latent variables. For the first such representation, we rely on results from Cadonna et al. (2020), where it is shown that marginalizing over  $\{\psi_{jt}\}$  leads to the following representation:

$$w_{jt}|\lambda_{jt}, c_j \sim t_{2c_j}(0, \theta_j \lambda_{jt}). \quad (14)$$

Therefore, the innovations conditional on  $\lambda_{jt}$  follow a Student- $t$  distribution with  $2c_j$  degrees of freedom. This representation also has direct implications for the choice of  $c_j$ , as the innovations  $w_{jt}$  conditional on  $\lambda_{jt}$  have no moments if  $c_j \leq 0.5$ . If  $c_j > 0.5$ , the conditional innovations have expectation zero, and when  $c_j > 1$  they additionally have finite variance. From this it can be inferred that a smaller  $c_j$  will lead to a process which allows for larger changes in the states a priori, whereas a larger  $c_j$  will cause the changes in the states to be more regularized. This interpretation is in line with the effect of  $c^\xi$  in the static triple gamma.

Further insights into the behavior of the dynamic triple gamma can be gleaned by examining the transition density  $p(\psi_{jt}|\psi_{j,t-1}, a_j, c_j, \rho_j)$  derived under the assumption that  $\lambda_{j,t-1}$  comes from the stationary distribution. This density is available in closed, albeit not well-known, form in Theorem 1. It allows for impulse response analysis, showcasing how the dynamic system responds to a shock while in the steady state. The proof can be found in Appendix C.

**Theorem 1.** *For the dynamic triple gamma prior defined in (8)-(11), with  $a_j > 0$ ,  $c_j > 0$ ,  $0 < \rho_j < 1$ , and  $\lambda_{j,t-1} \sim \mathcal{G}\left(a_j, \frac{a_j}{c_j}\right)$ , the following holds:*

$$\begin{aligned} p(\psi_{jt}|\psi_{j,t-1}, a_j, c_j, \rho_j) = & \\ & {}_2F_1\left(a_j + c_j, a_j + c_j, a_j, \frac{a_j^2 \rho_j \psi_{jt} \psi_{j,t-1}}{(a_j \psi_{jt} + c_j(1 - \rho_j))(a_j \psi_{j,t-1} + c_j(1 - \rho_j))}\right) \\ & \times \left(\frac{c_j^2 \left(\frac{a_j}{c_j} + \frac{1}{\psi_{j,t-1}}\right) (1 - \rho_j) \psi_{j,t-1}}{\left(c_j + \frac{a_j \psi_{jt}}{1 - \rho_j}\right) (a_j \psi_{j,t-1} + c_j(1 - \rho_j))}\right)^{a_j + c_j} \left(\frac{a_j}{c_j(1 - \rho_j)}\right)^{a_j} \frac{\psi_{jt}^{a_j - 1}}{B(a_j, c_j)}, \end{aligned} \quad (15)$$

where  ${}_2F_1(a, b, c; z)$  is the (Gaussian or ordinary) hypergeometric function

$${}_2F_1(a, b, c; z) = \sum_{n=0}^{\infty} \frac{(a)_n (b)_n}{(c)_n} \frac{z^n}{n!}, \quad (16)$$

and  $(q)_n$  are the rising factorials (a.k.a the Pochhammer function):

$$(q)_n = \begin{cases} 1 & n = 0, \\ \frac{\Gamma(q+n)}{\Gamma(q)} & n > 0. \end{cases} \quad (17)$$

Theorem 1 is useful both for building understanding of the properties of the dynamic triple gamma prior, as well as for the MCMC algorithm presented in Section 3. Figure 3 plots the transition density for various values of  $\rho_j$ ,  $c_j$  and  $\psi_{j,t-1}$ , highlighting the role both hyperparameters play in determining



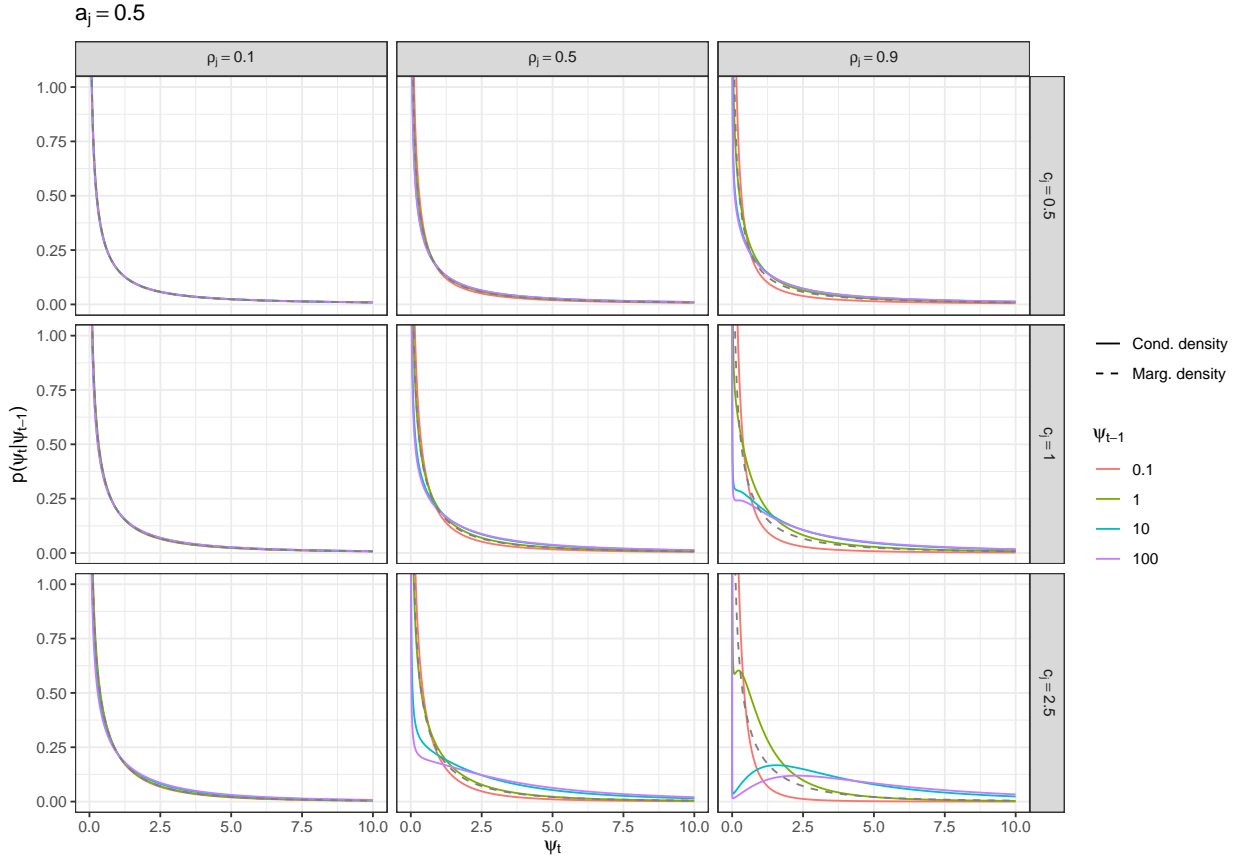


Figure 3: Transition density  $p(\psi_{jt}|\psi_{j,t-1}, a_j, c_j, \rho_j)$  under the assumption that  $\lambda_{j,t-1}$  comes from the stationary distribution for  $a_j = 0.5$  and  $c_j \in \{0.5, 1, 3\}$ . Colored lines represent transition densities for different values of  $\psi_{j,t-1}$ , while the grey dashed represents the marginal density.

the dynamic shrinkage characteristics of the DTG. Starting with  $\rho_j$ , one can see that the degree to which the density deviates from the marginal density for large values of  $\psi_{j,t-1}$  depends strongly on the value of  $\rho_j$ , with values closer to 1 corresponding to stronger deviation. Whereas all densities in the left-most column, where  $\rho_j = 0.1$ , hew closely to the marginal distribution, there exists significant variation in the right-most column, where  $\rho_j = 0.9$ . Despite this, it is interesting to note that the small value of  $a_j$  still causes all distributions to feature an infinite pole at the origin, irrespective of the value of  $\psi_{j,t-1}$ , with some distributions displaying multimodal behavior. This effect of  $\rho_j$  aligns with the idea of it being a parameter that controls autocorrelation, as, the larger  $\rho_j$  is, the more large values of  $\psi_{j,t-1}$  increase the probability of observing large values of  $\psi_{jt}$ .

Shifting focus to the effect of  $c_j$  reveals that, as in the static triple gamma,  $c_j$  controls the tails of the conditional density. Roughly speaking, smaller values of  $c_j$  lead to heavier tails, an idea that is also reflected in the fact that the marginal distribution has no moments for  $c_j < 0.5$ . This idea is extended to  $p(\psi_{jt}|\psi_{j,t-1}, a_j, c_j, \rho_j)$  in Theorem 2, with the proof again found in Appendix C.

**Theorem 2.** For  $\psi_{jt}|\psi_{j,t-1}, a_j, c_j, \rho_j$  with density defined in Theorem 1 and  $a_j > 0, c_j > 1, 0 < \rho_j < 1$ ,



and  $\lambda_{j,t-1} \sim \mathcal{G}\left(a_j, \frac{a_j}{c_j}\right)$ , the following holds:

$$\mathbb{E}[\psi_{jt}|\psi_{j,t-1}, a_j, c_j > 1, \rho_j] = (1 - \rho_j) \frac{c_j}{c_j - 1} + \rho_j \frac{\psi_{j,t-1} c_j (a_j + c_j)}{(c_j + a_j \psi_{j,t-1})(c_j - 1)}. \quad (18)$$

The implications of Theorem 2 align neatly with the intuition gained from Figure 3. The expectation is a weighted average of the expected value of the marginal  $F(2a_j, 2c_j)$  distribution (which is equal to  $c_j/(c_j - 1)$ ) and an expression depending non-linearly on  $\psi_{j,t-1}$ . Therefore, it deviates further from the marginal expectation the closer  $\rho_j$  is to 1. The tail controlling behavior of  $c_j$  becomes apparent if one lets  $c_j$  approach 1 from above, as

$$\lim_{c_j \downarrow 1} \mathbb{E}[\psi_{jt}|\psi_{j,t-1}, a_j, c_j, \rho_j] = \infty.$$

On the other hand, the fact that values of  $c_j > 1$  imply heavier regularisation of the tails is also evident, as the expectation, while monotonically increasing in  $\psi_{j,t-1}$ , is not unbounded. Specifically,

$$\lim_{\psi_{j,t-1} \rightarrow \infty} \mathbb{E}[\psi_{jt}|\psi_{j,t-1}, a_j, c_j > 1, \rho_j] = \frac{c_j(a_j + c_j \rho_j)}{a_j(c_j - 1)}.$$

Another benefit of Theorem 1 is that it allows for the derivation of conditional shrinkage profiles, in the spirit of Carvalho et al. (2010). Letting  $\theta_j = 1$  for illustrative purposes, one can re-parameterize the conditional density of  $w_{jt}$  in the following way:

$$w_{jt}|\tau_{jt} \sim \mathcal{N}\left(0, \frac{1}{\tau_{jt}} - 1\right), \quad (19)$$

where  $\frac{1}{\tau_{jt}} - 1 = \psi_{jt} \Leftrightarrow \tau_{jt} = \frac{1}{1+\psi_{jt}}$ . Using the law of transformation of densities yields the following useful corollary:

**Corollary 2.1.** Let  $\tau_{jt} = \frac{1}{1+\psi_{jt}}$ , where  $\psi_{jt}|\psi_{j,t-1}, a_j, c_j, \rho_j$  is a random variable with density defined in Theorem 1 and  $a_j > 0, c_j > 0, 0 < \rho_j < 1$ , and  $\lambda_{j,t-1} \sim \mathcal{G}\left(a_j, \frac{a_j}{c_j}\right)$ , then

$$p(\tau_{jt}|\psi_{j,t-1}, a_j, c_j, \rho_j) = p_{\psi_{jt}|\psi_{j,t-1}}\left(\frac{1}{\tau_{jt}} - 1\right) \frac{1}{\tau_{jt}^2}, \quad (20)$$

where  $p_{\psi_{jt}|\psi_{j,t-1}}(x)$  is shorthand for the transition density defined in (15).

$\tau_{jt}$  is confined to the range  $(0, 1)$  and characterizes the shrinkage behavior, with  $\tau_{jt}$  close to 1 implying “total” shrinkage, as the variance of  $w_{jt}$  then approaches 0 and  $\tau_{jt}$  close to 0 implying the opposite. Figure 4 graphs the dynamic shrinkage profiles for various values of  $\rho_j, c_j$  and  $\psi_{j,t-1}$ . The role of  $\rho_j$  as the parameter determining the extent to which the conditional distribution deviates from the marginal distribution is again readily apparent. Similarly,  $c_j$ 's importance for the shape of the tails of the distribution is reinforced. In the top row, where  $c_j = 0.5$ , the result is a dynamic horseshoe, with infinite poles in both corners, irrespective of the magnitude of  $\psi_{j,t-1}$ , with larger values of  $\psi_{j,t-1}$  allocating more prior mass towards 0 and vice versa.

In the bottom two rows, where  $1 \leq c_j$ , the infinite pole in the left corner disappears, implying some regularization in the tails, even for large values of  $\psi_{j,t-1}$ . This lines up nicely with the results derived from Theorem 2, as the expected value of the conditional density only exists for  $c_j > 1$ .

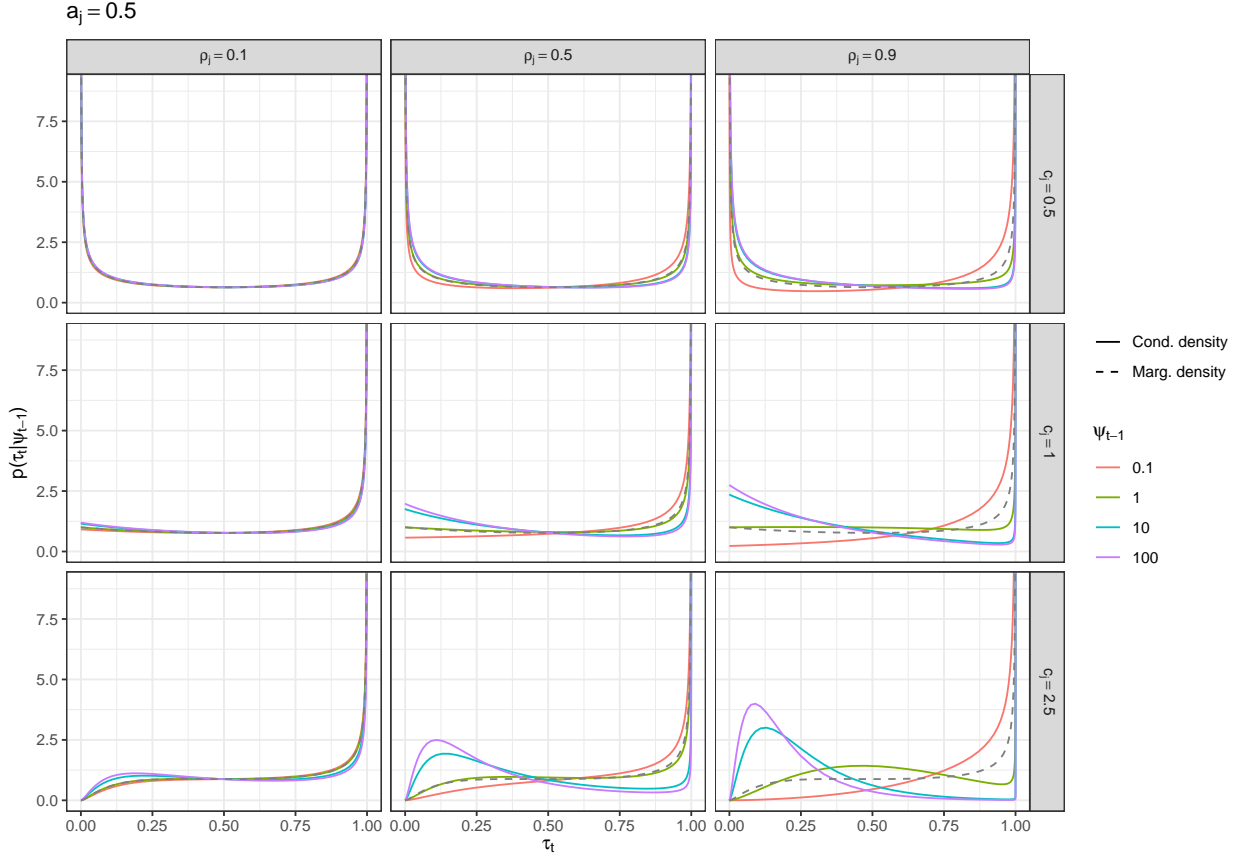


Figure 4: Dynamic shrinkage profiles  $p(\tau_{jt} | \psi_{j,t-1}, a_j, c_j, \rho_j)$  for  $a_j = 0.5$  and  $c_j \in \{0.5, 1, 2.5\}$ . Colored lines represent shrinkage profiles for different values of  $\psi_{j,t-1}$ , while the grey dashed represents the marginal shrinkage profile.

## 2.2 Relationship of the dynamic triple gamma to other approaches

The dynamic triple gamma shares a particularly close connection to two approaches previously proposed in the literature. First, the normal-gamma autoregressive (NGAR) process of [Kalli and Griffin \(2014\)](#) uses essentially the same recursive process as defined by (10)-(11), albeit with a different parameterization. Through this, they define a process directly on the  $\beta_{jt}$ 's, such that the resulting marginal distribution is a normal-gamma shrinkage prior ([Griffin and Brown, 2010](#)). This leads to a strictly stationary process for the  $\beta_{jt}$ 's. In contrast to this, the proposed approach defines a process that is marginally triple gamma on the *innovations* (i.e. the  $w_{jt}$ 's) and not on the states themselves, which are therefore allowed to follow a non-stationary process.

Second, there exists a (slightly less obvious) connection to the dynamic shrinkage process proposed by [Kowal et al. \(2019\)](#), where autocorrelation is induced in the innovations through an AR(1) process on the log of the innovation variance:

$$w_{jt} | h_{jt} \sim \mathcal{N}(0, e^{h_{jt}}), \quad h_{jt} = \phi_j^h (h_{j,t-1} - \mu_j^h) + \eta_{jt}, \quad \eta_{jt} \sim \mathcal{Z}(a_j, c_j, \mu_j^h, 1), \quad (21)$$

where the  $\eta_{jt}$  arise from a Z-distribution and  $\phi_j^h$  acts as an autocorrelation parameter.

To see how the proposed approach and that of [Kowal et al. \(2019\)](#) are related, note that the triple gamma prior can, following [Cadonna et al. \(2020\)](#), also be represented as:

$$w_{jt}|\tilde{\psi}_{jt}, a_j, c_j, \theta_j \sim \mathcal{N}\left(0, \phi_j \tilde{\psi}_{jt}\right), \quad \tilde{\psi}_{jt}|a_j, c_j \sim \mathcal{BP}(a_j, c_j), \quad (22)$$

where

$$\tilde{\psi}_{jt} = \frac{a_j}{c_j} \psi_{jt}, \quad \phi_j = \frac{2c_j}{\kappa_j a_j} = \theta_j \frac{c_j}{a_j}, \quad (23)$$

and  $\mathcal{BP}(a_j, c_j)$  is the beta-prime distribution<sup>2</sup>. Based on this, it is possible to verify the following new representation of the triple gamma:

$$w_{jt}|h_{jt} \sim \mathcal{N}\left(0, e^{h_{jt}}\right), \quad h_{jt}|a_j, c_j, \theta_j \sim \mathcal{Z}(a_j, c_j, \log \phi_j, 1). \quad (24)$$

Specifically, from representation (22) we find that  $h_{jt} = \log \phi_j + \log \tilde{\psi}_{jt}$ , where  $\tilde{\psi}_{jt} \sim \mathcal{BP}(a_j, c_j)$ . It is easy to verify that

$$X \sim \mathcal{BP}(a, c) \Leftrightarrow Y = \log X \sim \mathcal{Z}(a, c, 0, 1).$$

From

$$Y \sim \mathcal{Z}(a, c, 0, 1) \Leftrightarrow Y + \mu \sim \mathcal{Z}(a, c, \mu, 1),$$

it follows that  $h_{jt}|a_j, c_j, \theta_j \sim \mathcal{Z}(a_j, c_j, \log \phi_j, 1)$ .

Essentially, the conditional distribution of  $w_{jt}^2|a_j, c_j, \theta_j$  proposed by [Kowal et al. \(2019\)](#) is equivalent to the triple gamma prior. This result is already interesting on its own, as it allows the properties of the triple gamma derived in [Cadonna et al. \(2020\)](#) to shed light on the characteristics of the dynamic shrinkage process. It further implies that the two approaches coincide when the respective autocorrelation parameters ( $\rho_j$  and  $\phi_j^h$ ) are equal to 0, as they both result in squared innovations that are i.i.d. triple gamma. The key difference is that the marginal form of the proposed approach is again well-known, i.e. triple gamma. This allows the shrinkage characteristics of the entire process to be better understood, while sacrificing some tractability of the conditional distribution. There are also computational advantages, as the MCMC algorithm proposed in Section 3 does not need to rely on mixture approximations, which tend to be expensive to evaluate.

### 2.3 Hyperprior choices

Before computation can be discussed, hyperprior choices need to be made for the various hyperparameters. First and foremost, we follow [Cadonna et al. \(2020\)](#) and place static triple gamma prior distributions on both  $\beta_j^2 \sim TG(a^\tau, c^\tau, \lambda_B^2)$  and  $\theta_j \sim TG(a^\xi, c^\xi, \kappa_B^2)$ . As  $\theta_j$  acts as the global shrinkage parameter and  $\beta_j$  is the mean of the initial value of state  $\{\beta_{jt}\}$ , this prior setup allows the model to effectively differentiate between time-varying, static and excluded covariates. Further, we place scaled beta priors on  $a^\tau, a^\xi, c^\tau$  and  $c^\xi$ :

$$2a^\xi \sim \mathcal{B}(\alpha_{a^\xi}, \beta_{a^\xi}), \quad 2c^\xi \sim \mathcal{B}(\alpha_{c^\xi}, \beta_{c^\xi}), \quad 2a^\tau \sim \mathcal{B}(\alpha_{a^\tau}, \beta_{a^\tau}), \quad 2c^\tau \sim \mathcal{B}(\alpha_{c^\tau}, \beta_{c^\tau}). \quad (25)$$

<sup>2</sup>For details on the non-standard distributions used in this section see Appendix A.

This ensures that all shape parameters remain in the range  $(0, 0.5)$ , thereby preserving the strong pole around the origin as well as the heavy tails.

We further follow the arguments in [Cadonna et al. \(2020\)](#) and place scaled F priors on the global shrinkage parameters  $\lambda_B^2$  and  $\kappa_B^2$ . Specifically,

$$\frac{\kappa_B^2}{2} \mid a^\xi, c^\xi \sim F(2a^\xi, 2c^\xi), \quad \frac{\lambda_B^2}{2} \mid a^\tau, c^\tau \sim F(2a^\tau, 2c^\tau). \quad (26)$$

For the prior on  $\sigma_t^2$ , two cases have to be differentiated. In the homoscedastic  $\sigma_t^2 = \sigma^2$  case, we place a hierarchical prior on  $\sigma^2$ , where the scale of an inverse gamma follows a gamma distribution:

$$\sigma^2 \mid C_0 \sim \mathcal{G}^{-1}(c_0, C_0), \quad C_0 \sim \mathcal{G}(g_0, G_0), \quad (27)$$

with hyperparameters  $c_0$ ,  $g_0$ , and  $G_0$ . In the case of stochastic volatility, we follow [Kastner and Frühwirth-Schnatter \(2014\)](#) in the choice of priors on the parameters  $\mu$ ,  $\phi$  and  $\sigma_\eta^2$  in Equation (3):

$$\mu \sim \mathcal{N}(b_\mu, B_\mu), \quad \frac{\phi + 1}{2} \sim \mathcal{B}(a_\phi, b_\phi), \quad \sigma_\eta^2 \sim \mathcal{G}(1/2, 1/2B_\sigma), \quad (28)$$

with hyperparameters  $b_\mu$ ,  $B_\mu$ ,  $a_\phi$ ,  $b_\phi$ , and  $B_\sigma$ .

Finally, a prior has to be specified for  $\rho_j$ . Here, we incorporate insights from [Gourieroux and Jasiak \(2006\)](#), where it is shown that the stochastic process degenerates as  $\rho_j$  approaches 1. To avoid this, we place a generalized beta prior of the first kind (GB1) on  $\rho_j$ , which has density function

$$f(\rho_j; a_\rho, b_\rho, \alpha_\rho, \beta_\rho) = \frac{|a_\rho| \rho_j^{a_\rho \alpha_\rho - 1} (1 - (\rho_j/b_\rho)^{a_\rho})^{\beta_\rho - 1}}{b_\rho^{a_\rho \alpha_\rho} B(\alpha_\rho, \beta_\rho)}, \quad (29)$$

for  $0 < \rho_j < b_\rho$  and  $a_\rho \in \mathbb{R}$ ,  $b_\rho > 0$ ,  $\alpha_\rho > 0$ , and  $\beta_\rho > 0$ . It generalizes the beta distribution in two ways. First, it allows the support of the distribution to range from 0 to  $b_\rho$ ; second, the parameter  $a_\rho$  determines the power to which the argument is taken. For the purposes of bounding the prior away from 1, the former property is more important, as one can limit the support of the prior. For example, in the application in Section 4, we set  $b_\rho = 0.95$ , thereby restricting support to the range  $(0, 0.95)$ .

### 3 MCMC estimation

Sampling all unknown variables from the posterior of the DTG prior is challenging both from a theoretical as well as a computational perspective. These challenges stem almost exclusively from the  $\psi_{jt}$ 's and the associated hyperpriors, which becomes evident when noting that the model simplifies to a linear Gaussian state space model when conditioning on the  $\psi_{jt}$ 's. As this is a well-understood class of models, we can fall back on algorithms that are fairly standard in the literature for the portions of the MCMC algorithm that deal with a conditionally Gaussian state space model. This includes, for example, the simulation smoother of [McCausland et al. \(2011\)](#) or the ancillarity-sufficiency interweaving strategy (ASIS) of [Yu and Meng \(2011\)](#) to increase the sampling efficiency of  $\theta_1, \dots, \theta_d$ . Therefore, we focus on the parts of the algorithm that are non-standard here, by assuming that the innovations  $w_{jt} = \beta_{jt} - \beta_{j,t-1}$  are known. We give a full overview of the MCMC scheme in Appendix D.

### 3.1 Sampling under *a priori* independent innovations

To give an intuitive understanding of the MCMC sampler, we begin by discussing how to draw samples from the simplest model, characterized by *a priori* independent triple gamma innovations, i.e.  $w_{jt}|\theta_j, a_j, c_j \stackrel{\text{iid}}{\sim} TG(a_j, c_j, 2/\theta_j)$ , which results as a special case of the DTG when  $\rho_j = 0$ . Here, one can employ either the sampler proposed in Cadonna et al. (2020) or, based on representation (12), utilize a generalized and innovative version of the sampler introduced for the horseshoe by Makalic and Schmidt (2016). Applying standard derivations for conditionally conjugate densities involving the inverse gamma and gamma distributions yields:

$$\psi_{jt}|w_{jt}, \lambda_{jt}, \theta_j, c_j \sim \mathcal{G}^{-1}\left(c_j + \frac{1}{2}, \frac{w_{jt}^2}{2\theta_j} + \lambda_{jt}\right), \quad (30)$$

$$\lambda_{jt}|\psi_{jt}, a_j, c_j \sim \mathcal{G}\left(a_j + c_j, \frac{a_j}{c_j} + \frac{1}{\psi_{jt}}\right), \quad (31)$$

for  $t = 1, \dots, T$  and  $j = 1, \dots, d$ . This result is valuable in its own right, offering a method for sampling from the posterior of a model under the triple gamma prior without relying on the generalized inverse Gaussian distribution (GIG) as in Cadonna et al. (2020). As the GIG is not as widely implemented in programming languages compared to the gamma and inverse gamma distributions, this outcome facilitates the broader application of the triple gamma prior.

### 3.2 Sampling for fixed $\rho_j$

Moving from the case where the innovations are i.i.d. triple gamma, the next simplest case is one where autocorrelation is modeled via a fixed  $\rho_j$ . Here, the hierarchical structure allows a fairly straightforward Gibbs sampler to be implemented to sample from the posterior of the parameters. The conditional density (30) for  $\psi_{jt}$  does not require any modification, as conditional on  $\lambda_{jt}$ , it is independent of  $\kappa_{j1}, \dots, \kappa_{jT}$ . The full conditional posterior for  $\lambda_{jt}$  can, once again, be found through fairly standard derivations based on gamma and inverse gamma densities:<sup>3</sup>

$$\lambda_{jt}|\psi_{jt}, \kappa_{jt}, \kappa_{j,t+1}, a_j, c_j, \rho_j \sim \mathcal{G}\left(a_j + c_j + \kappa_{jt} + \kappa_{j,t+1}, \frac{a_j}{c_j} \frac{1 + \rho_j}{1 - \rho_j} + \frac{1}{\psi_{jt}}\right), \quad (32)$$

where the independence case  $\rho_j = 0$  leads back to (31).  $\kappa_{jt}|\lambda_{jt}, \lambda_{j,t-1}, a_j, c_j, \rho_j$  follows a discrete distribution, independently of all other state variables, with weights given by:

$$\Pr(\kappa_{jt} = k|\lambda_{jt}, \lambda_{j,t-1}, a_j, c_j, \rho_j) \propto p_{jk}(\lambda_{jt}\lambda_{j,t-1})^k, \quad p_{jk} = \left(\frac{a_j\sqrt{\rho_j}}{c_j(1-\rho_j)}\right)^{2k} \frac{1}{\Gamma(a_j+k)\Gamma(k+1)}. \quad (33)$$

Sampling in this fully conditional setup works well, with good mixing and computations that are able to be performed fairly quickly. However, fixing  $\rho_j$  a priori is a fairly strong assumption, particularly because it has a large influence on the properties of the DTG (see Section 2.1).

---

<sup>3</sup>In several of the sampling steps discussed in this section, adjustments are necessary for the cases where  $t \in \{0, 1, T\}$ .

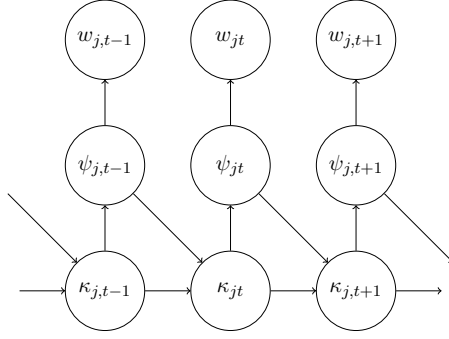


Figure 5: Interdependencies of the latent variables of the dynamic triple gamma prior represented as a directed graph, in the alternate state space model defined by (35) together with (36) and (37).

### 3.3 Sampling with unknown $\rho_j$

As opposed to the sampling steps for  $\psi_{jt}$ ,  $\lambda_{jt}$  and  $\kappa_{jt}$ , the full conditional posterior of  $\rho_j$  is not available in closed form, necessitating the use of a Metropolis-Hastings-within-Gibbs step. Implementing such a step within a fully conditional Gibbs loop in a straightforward fashion leads to poor mixing. To alleviate this issue, we make use of marginalization, using various representations of the hierarchical structure with different sets of random variables marginalized out.

For the Metropolis-Hastings (MH) step of  $\rho_j$  itself, we construct an approximate likelihood using Theorem 1:

$$p(\psi_{j1}, \dots, \psi_{jT} | \rho_j, a_j, c_j) \approx p(\psi_{j1} | a_j, c_j, \rho_j) \prod_{t=2}^T p(\psi_{jt} | \psi_{j,t-1}, a_j, c_j, \rho_j), \quad (34)$$

where  $p(\psi_{jt} | \psi_{j,t-1}, a_j, c_j, \rho_j)$  is the density defined in (15). This, combined with the prior density defined in Section 2.3, gives us the posterior up to an unknown constant, allowing the construction of an MH step to generate samples from the conditional posterior. The important thing to note here is that this approximate likelihood is marginalized w.r.t.  $\lambda_{j1}, \dots, \lambda_{jT}$  and  $\kappa_{j1}, \dots, \kappa_{jT}$ . Thus, to preserve the stationary distribution of the Markov chain, one needs to sample either  $\lambda_{j1}, \dots, \lambda_{jT}$  or  $\kappa_{j1}, \dots, \kappa_{jT}$  from densities that are marginalized w.r.t. to the respective other (van Dyk and Park, 2008).

It is possible to construct a state space model with the same marginal properties as the one introduced in Section 2, albeit with  $\lambda_{jt}, \dots, \lambda_{jT}$  marginalized out. It is characterized by a generalized beta prime transition density for  $\psi_{jt} | \kappa_{jt}, a_j, c_j, \rho_j$ , specifically

$$\psi_{jt} | \kappa_{jt}, a_j, c_j, \rho_j \sim \mathcal{BP} \left( a_j + \kappa_{jt}, c_j, 1, \frac{c_j(1 - \rho_j)}{a_j} \right), \quad (35)$$

coupled with the following negative binomial transition density for  $\kappa_{jt} | \kappa_{j,t-1}, \psi_{j,t-1}, \rho_j, a_j, c_j$ :

$$\begin{aligned} \kappa_{jt} | \kappa_{j,t-1}, \psi_{j,t-1}, \rho_j, a_j, c_j &\sim \text{NegBin}(a_j + c_j + \kappa_{j,t-1}, \pi_{j,t-1}), \\ \pi_{j,t-1} &= \frac{a_j \psi_{j,t-1} + c_j(1 - \rho_j)}{(1 + \rho_j) a_j \psi_{j,t-1} + c_j(1 - \rho_j)}, \end{aligned} \quad (36)$$

with the initial value coming from the stationary distribution:

$$\kappa_{j1}|a_j, \rho_j \sim \text{NegBin}(a_j, 1 - \rho_j). \quad (37)$$

A representation of the interdependencies of this partially marginalized state space model as a directed graph can be found in Figure 5. Details on the derivations required to arrive at the transition densities can be found in Appendix B.

In this alternate state space representation, we can now sample  $\kappa_{j1}, \dots, \kappa_{jT}$  conditional on  $\psi_{j1}, \dots, \psi_{jT}$  but marginalized w.r.t.  $\lambda_{j1}, \dots, \lambda_{jT}$ , thereby preserving the ergodic distribution of the Markov chain. More specifically

$$\begin{aligned} & p(\kappa_{jt}|\kappa_{j,t-1}, \kappa_{j,t+1}, \psi_{jt}, \psi_{j,t-1}, \rho_j, a_j, c_j) \\ \propto & \frac{\Gamma(a_j + c_j + \kappa_{j,t-1} + \kappa_{jt})\Gamma(a_j + c_j + \kappa_{jt} + \kappa_{j,t+1})}{\kappa_{jt}!\Gamma(a_j + \kappa_{jt})} \left[ (1 - \pi_{j,t-1})\pi_{jt} \frac{a_j\psi_{jt}}{a_j\psi_{jt} + c_j(1 - \rho_j)} \right]^{\kappa_{jt}}, \end{aligned} \quad (38)$$

with  $\pi_{j,t-1}$  defined as in (36).

Further, it can be shown that the normalizing constant of this distribution is available in closed form. To this end, note that, from the definition of the hypergeometric function presented in (16) and (17), it follows immediately that following infinite series can be represented by a hypergeometric function:

$$\sum_{k=0}^{\infty} \frac{\Gamma(a+k)\Gamma(b+k)}{\Gamma(c+k)} \frac{z^k}{k!} = \frac{\Gamma(a)\Gamma(b)}{\Gamma(c)} {}_2F_1(a, b; c; z).$$

Therefore, the normalizing constant of (38) is equal to

$$\sum_{\kappa_{jt}=0}^{\infty} p(\kappa_{jt}|\kappa_{j,t-1}, \kappa_{j,t+1}, \psi_{jt}, \psi_{j,t-1}, \rho_j, a_j, c_j) = \frac{\Gamma(a_{jt}^{\kappa})\Gamma(b_{jt}^{\kappa})}{\Gamma(a_j)} {}_2F_1\left(a_{jt}^{\kappa}, b_{jt}^{\kappa}; a_j; \frac{\rho_j\pi_{j1}a_j\psi_{j1}}{a_j\psi_{j1} + c_j(1 - \rho_j)}\right), \quad (39)$$

with  $a_{jt}^{\kappa} = a_j + c_j + \kappa_{j,t-1}$  and  $b_{jt}^{\kappa} = a_j + c_j + \kappa_{j,t+1}$ .

Based on the normalized weights defined by (38) and (39), two main options present themselves to sample  $\kappa_{jt}$ . One could adapt Algorithm 11.5 in Frühwirth-Schnatter (2006, p.342), to derive a forward-filtering-backward-sampling (FFBS) algorithm for  $\kappa_{jt}$ . This re-frames  $\kappa_{jt}$  as a hidden Markov chain with  $K_{\max}$  hidden states, with the entries of its transition matrix  $\xi_t$  given by the normalized version of (38). The theoretical attractiveness of this approach lies in the ability to draw from the joint distribution of  $\kappa_{j1}, \dots, \kappa_{jT}$ , thereby improving mixing. The downside of this approach is that it requires the computation of all  $K_{\max}^2 \times (T - 1)$  transition matrices before sampling can be performed, which becomes fairly computationally demanding for even moderately sized problems.

An alternate approach consists of sampling  $\kappa_{jt}$  directly using inverse transform sampling and the probabilities defined by (38) and (39). The probabilities have a convenient recursive structure (see Appendix D), allowing for efficient computation, as only the probabilities up to the current realization of  $\kappa_{jt}$  need to be evaluated for inverse transform sampling to work. Thus, particularly when many values of  $\kappa_{jt}$  are zero or near zero (as is the case with heavy shrinkage), this method can be executed orders of magnitude faster than FFBS. Further, we found that mixing was fairly good when using this method,

---

To maintain brevity, these modifications can be found in Appendix D.



despite it being a single move sampler. As a result of its superior speed and generally favorable mixing, we advocate for adopting this method to sample  $\kappa_{jt}$ .

In summary, the proposed sampler aims to alleviate poor mixing for  $\rho_j$  by using the approximate likelihood (34) marginalized w.r.t.  $\lambda_{jt}, \dots, \lambda_{jT}$  and  $\kappa_{jt}, \dots, \kappa_{jT}$  to construct a collapsed MH-within-Gibbs step for  $\rho_j$ . To preserve the ergodic distribution of the Markov chain, it is then necessary to move to a partially marginalized state space model and sample  $\kappa_{j1}, \dots, \kappa_{jT}$  conditional on  $\psi_{j1}, \dots, \psi_{jT}$  but marginalized w.r.t.  $\lambda_{j1}, \dots, \lambda_{jT}$ . This is done by applying inverse transform sampling to the normalized version of (38). Next, one can sample  $\lambda_{jt}, \dots, \lambda_{jT}$  as in the fixed  $\rho_j$  case, as defined by (32). Finally, conditional on  $\lambda_{jt}, \dots, \lambda_{jT}, \psi_{j1}, \dots, \psi_{jT}$  can be sampled as in the *a priori* i.i.d. innovations case, defined by (30). It is important to note that the sampling order is important when marginalizing out random variables, as the stationary distribution of the Markov chain is not invariant to permutations of the sampling steps.

## 4 Application

### 4.1 The Cholesky SV-model

The Cholesky SV-model developed by Lopes et al. (2016) and further refined by Bitto and Frühwirth-Schnatter (2019) provides a method for modeling sparse, time-varying variance-covariance matrices  $\Sigma_t$ , for  $t = 1, \dots, T$ , of an  $M$ -dimensional multivariate time series that follows a conditionally zero mean normal distribution, i.e.  $\mathbf{y}_t | \Sigma_t \sim \mathcal{N}_M(\mathbf{0}, \Sigma_t)$ . The key ingredient is the decomposition  $\Sigma_t = \mathbf{\Lambda}_t \mathbf{D}_t \mathbf{\Lambda}_t'$ , where  $\mathbf{\Lambda}_t$  is lower unitriangular and  $\mathbf{D}_t$  is a diagonal matrix. As a consequence,  $\mathbf{\Lambda}_t^{-1} \mathbf{y}_t \sim \mathcal{N}_M(\mathbf{0}, \mathbf{D}_t)$ , which, letting the elements of  $\mathbf{\Lambda}_t^{-1}$  be denoted as  $\gamma_{ij,t}$  for  $j < i$ , can be expressed as

$$\begin{bmatrix} 1 & \dots & & & 0 \\ \gamma_{21,t} & 1 & & & 0 \\ & & \ddots & & 0 \\ \vdots & & & 1 & 0 \\ \gamma_{M1,t} & \gamma_{M2,t} & \dots & \gamma_{M,M-1,t} & 1 \end{bmatrix} \begin{bmatrix} y_{1t} \\ y_{2t} \\ \vdots \\ y_{Mt} \end{bmatrix} \sim \mathcal{N}_M(\mathbf{0}, \mathbf{D}_t).$$

This, in turn, can be represented as a series of independent regression equations, as  $\mathbf{D}_t$  is a diagonal matrix:

$$\begin{aligned} y_{1t} &= \varepsilon_{1t}, & \varepsilon_{1t} &\sim \mathcal{N}(0, \sigma_{1t}^2), \\ y_{2t} &= -\gamma_{21,t} y_{1t} + \varepsilon_{2t}, & \varepsilon_{2t} &\sim \mathcal{N}(0, \sigma_{2t}^2), \\ y_{3t} &= -\gamma_{31,t} y_{1t} - \gamma_{32,t} y_{2t} + \varepsilon_{3t}, & \varepsilon_{3t} &\sim \mathcal{N}(0, \sigma_{3t}^2), \\ & \vdots & & \\ y_{Mt} &= -\gamma_{M1,t} y_{1t} - \dots - \gamma_{M,M-1,t} y_{M-1,t} + \varepsilon_{Mt}, & \varepsilon_{Mt} &\sim \mathcal{N}(0, \sigma_{Mt}^2). \end{aligned}$$

To further allow for conditional heteroscedasticity, one can let the  $\sigma_{jt}^2 = e^{h_{jt}}$  follow a stochastic volatility law of motion, as defined in (3).

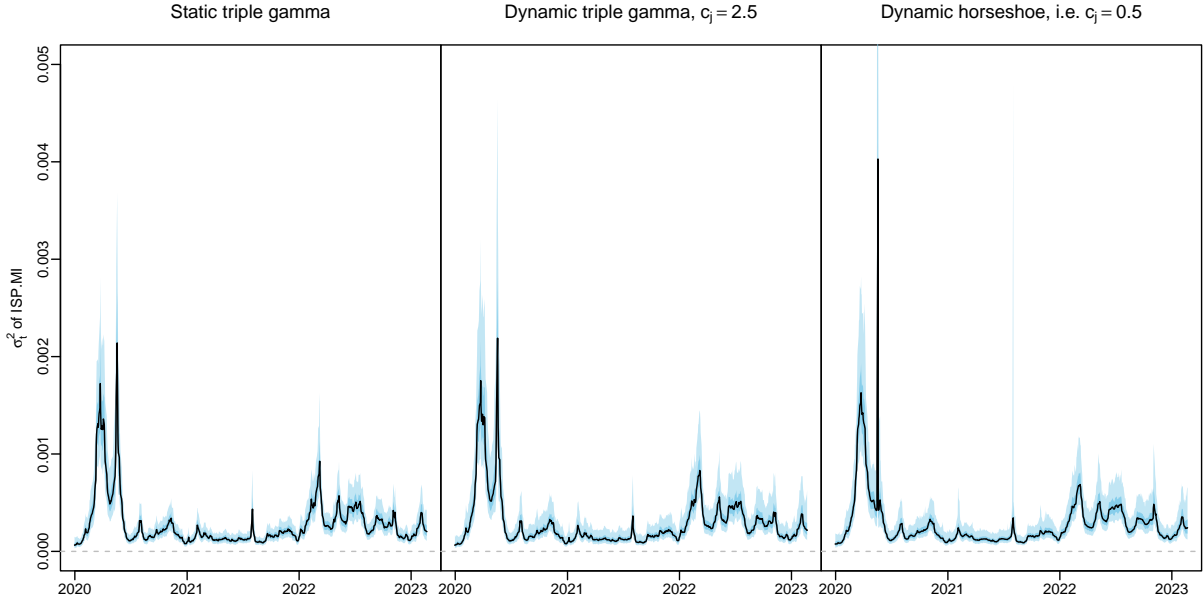


Figure 6: Estimated marginal variance of returns of Intesa Sanpaolo in a Cholesky SV-model under the static triple gamma prior, dynamic triple gamma and dynamic horseshoe. The black line represents the posterior median, while the blue shaded regions represent the pointwise 90% and 50% credible intervals.

The equations above can now be estimated as a series of independent TVP regression models, as defined in (6)-(7), where the  $\gamma_{mj,t}$  (and hence also the  $\Lambda_t$ ) can be recovered from the regression coefficients as  $-\beta_{mj,t}$ . The idiosyncratic variance matrix  $D_t$  can be recovered from the estimated paths of the log volatilities of the individual equations as  $D_t = \text{Diag}(e^{h_{1t}}, \dots, e^{h_{Mt}})$ , with the exception of  $e^{h_{1t}}$ , for which, due to the absence of any regressors, a stochastic volatility model has to be estimated separately. Placing a dynamic triple gamma prior on the innovations of the regression coefficients allows for covariance modeling that is highly sparse, due to the strong shrinkage imposed by the prior, while still allowing for adaptation to locally different (co)variances, thanks to the inherently autoregressive structure of the DTG.

## 4.2 Application to the EURO STOXX 50 index

We apply the Cholesky SV-model equipped with the dynamic triple gamma prior to a data set of 45 out of 50 of the returns on the companies represented in the EURO STOXX 50 index (with 5 dropped due to data availability issues, see Appendix E for more detailed description). The order of the data set is alphabetical and it spans 810 time points from the 2nd of January, 2020 to the 21st of February, 2023. Due to the COVID-19 pandemic and the ensuing volatility in financial markets, this represents a particularly challenging data set for econometric modeling. We test two different choices of  $c_j$ , namely  $c_j = 0.5$  and  $c_j = 2.5$ , as the former implies a marginal horseshoe prior for the innovations with no moments and very heavy tails, while the latter allows for some regularization of the tails.  $a_j$  is set to 0.5 in both cases, as we still want to induce heavy shrinkage around the origin. In both setups, we use the GB1 prior for

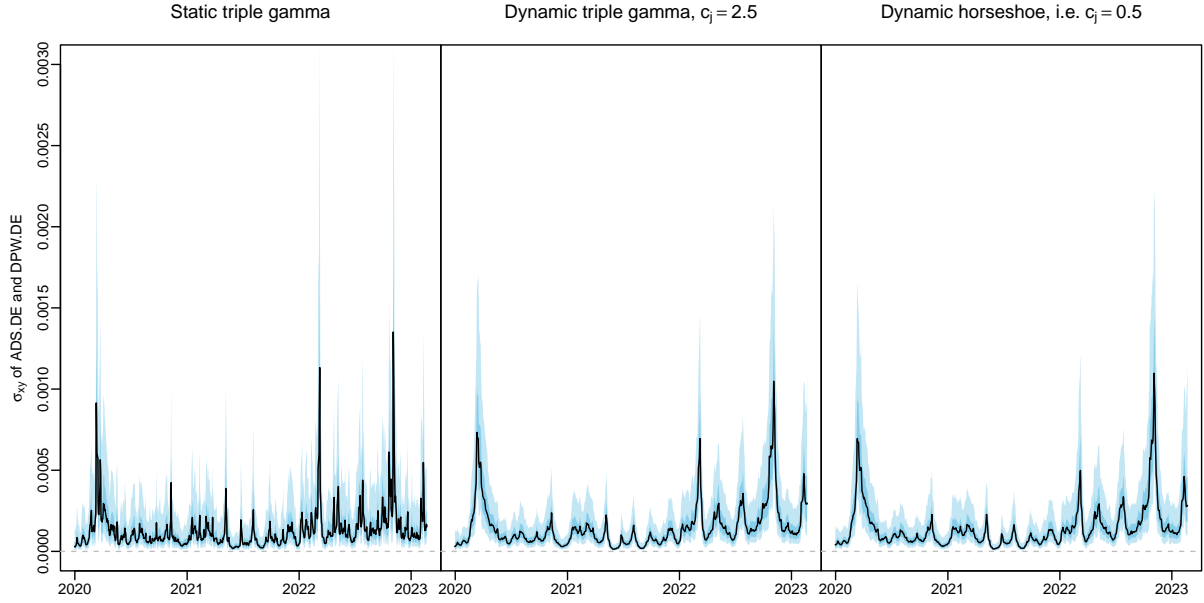


Figure 7: Estimated marginal covariance of returns of Adidas and Deutsche Post in a Cholesky SV-model under the static triple gamma prior, dynamic triple gamma and dynamic horseshoe. The black line represents the posterior median, while the blue shaded regions represent the pointwise 90% and 50% credible intervals.

$\rho_j$  defined in (29), with hyperparameters  $a_\rho = 1$ ,  $b_\rho = 0.95$ ,  $\alpha_\rho = 0.5$ , and  $\beta_\rho = 0.5$ . This results in a prior that has a horseshoe shape ranging from 0 to 0.95, incorporating the prior information that we either expect a state to display very little autocorrelation or a large amount of autocorrelation, but not a middling amount. For the global shrinkage parameters of the innovations as well as the means of the initial values we employ the static triple gamma prior distributions  $\beta_j^2 \sim TG(a^\tau, c^\tau, \lambda_B^2)$  and  $\theta_j \sim TG(a^\xi, c^\xi, \kappa_B^2)$ , under the hyperpriors defined in (25) and (26), with hyperparameters  $\alpha_{a\xi} = \alpha_{a\tau} = \alpha_{c\xi} = \alpha_{c\tau} = 5$ ,  $\beta_{a\xi} = \beta_{a\tau} = 10$  and  $\beta_{c\xi} = \beta_{c\tau} = 2$ . For the hyperparameters of the stochastic volatility equations, we use the default choices of Knaus et al. (2022). For comparison, we also estimate a Cholesky SV-model under a static, hierarchical triple gamma prior, using the default hyperparameters laid out in Knaus et al. (2021) and under the dynamic shrinkage process of Kowal et al. (2019), using the default hyperparameter values suggested by the authors. Each model was run for 100 000 iterations, with a burn-in of 20 000 and a thinning factor of 100.

Generally speaking, most elements of the estimated time varying variance-covariance matrix  $\Sigma_t$  are very close to zero for large stretches of time, with notable exceptions being early 2020 and early 2022. While all three prior specifications result in posterior estimates with this property, there exist two notable differences. First, the dynamic horseshoe displays large, sudden jumps followed by periods of relative calm, showcasing the flexibility of the dynamic triple gamma prior approach, as well as the heavy tails of the horseshoe prior. An example of this behavior can be seen in the third panel of Figure 6, in the first third of 2020. Second, the under-shrinking behavior of the static triple gamma approach becomes apparent in some estimated variances and covariances. To be able to accommodate the drastic changes

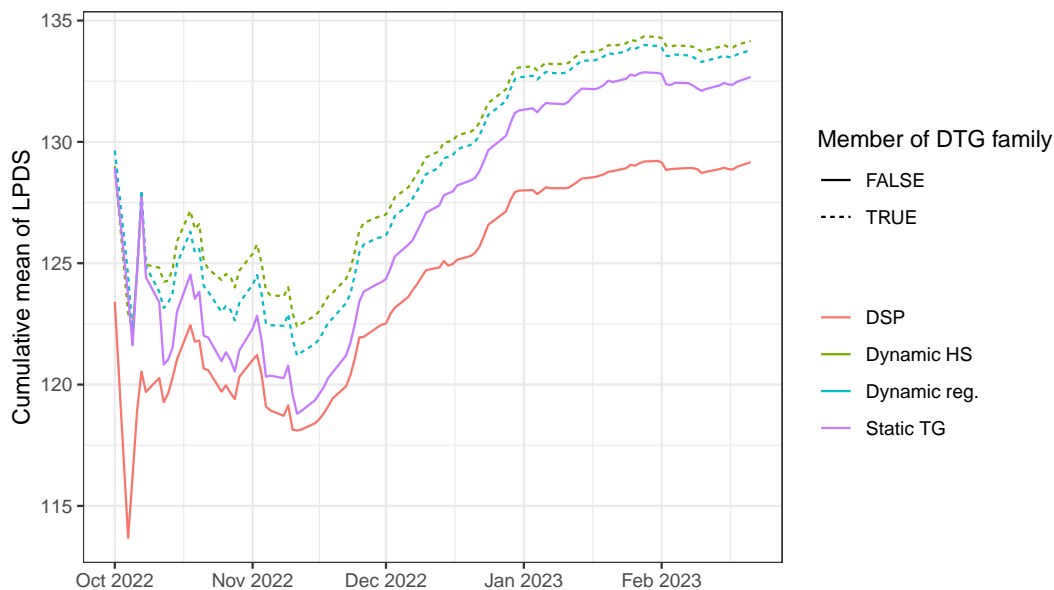


Figure 8: Cumulative mean of one step ahead log-predictive density scores for the last 100 time points of the EURO STOXX data under a static triple gamma (Static TG), dynamic triple gamma with  $c_j = 2.5$  (Dynamic reg.), a dynamic horseshoe (Dynamic HS) and the dynamic shrinkage process (DSP) of Kowal et al. (2019).

in the magnitude of the estimates, the associated  $\theta_j$  can become too large to effectively shrink noise in calmer periods. In contrast, the dynamic triple gamma can adapt to the locally differing variance requirements of a given state. An example of this can be seen in Figure 7, which displays the marginal time-varying covariance of two returns, where the estimate from the static approach is much noisier than that under either dynamic specification. High resolution images of all variance-covariance matrices can be found [here](#).<sup>4</sup>

#### 4.2.1 Comparing forecasting performance

To benchmark the out-of-sample forecasting performance of our approach, we compare the one step ahead log-predictive density scores (LPDS) for the last 100 time points in the data set. The cumulative mean of this exercise can be found in Figure 8. Both the slightly regularized dynamic triple gamma as well as the dynamic horseshoe outperform the static triple gamma, as is evidenced by the higher average LPDS throughout virtually the entire sample period. Furthermore, both the static and dynamic triple gamma priors clearly outperform the dynamic shrinkage process of Kowal et al. (2019). To gain intuition about how the dynamic triple gamma prior outperforms the static approach, it is instructive to look at Figure 9. It graphs the pointwise difference in LPDS vis-à-vis the static approach, for both the regularized dynamic triple gamma, as well as the dynamic horseshoe. It is interesting to note that the dynamic approaches forecasts better only in around 60% of time points. However, whenever the

<sup>4</sup>In case the link is not clickable: <https://imgur.com/a/xoiGkFb>

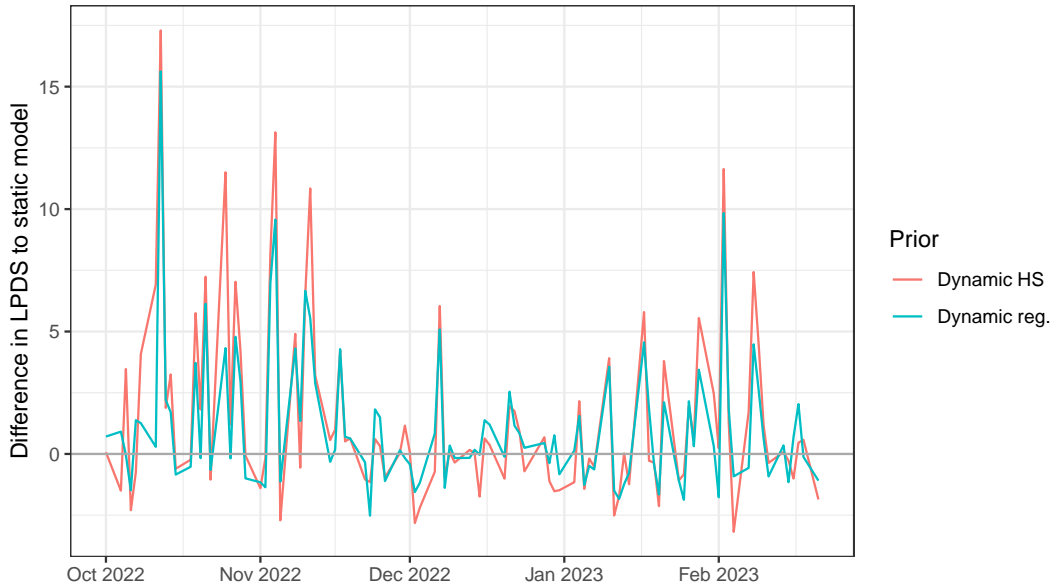


Figure 9: Difference in one step ahead log-predictive density score to static triple gamma prior for the last 100 time points of the EURO STOXX data under a dynamic triple gamma with  $c_j = 2.5$  (Dynamic reg.) and a dynamic horseshoe (Dynamic HS).

forecasting performance of the dynamic approach is worse than the static approach, it is usually not worse by much. In contrast, when the forecasting performance is better, it is often substantially so, leading to forecasting performance that is, on average, much better than under the static approach.

## 5 Concluding remarks

In this paper we presented a novel approach to dynamic sparsity, through a stochastic process that results in a marginal triple gamma distribution. This has the twofold advantage of being a well-understood marginal form with favorable shrinkage characteristics, while also allowing for the triple gamma’s many special and limiting cases to be implemented as marginal densities. As such, it is also the first stochastic process that can have the horseshoe prior as its marginal form while still allowing for autocorrelation. We derived many properties of the dynamic triple gamma, in particular through impulse response analysis, and used this to further argue that it is a good choice for dynamic sparsity. We developed an efficient MCMC algorithm to sample from the posterior, which scales well to medium-sized data sets, as the individual steps are all computationally cheap to evaluate. A Cholesky SV-model equipped with the dynamic triple gamma was fit to a data set of returns of companies that comprise the EURO STOXX 50 index, where it was shown that it is able to effectively induce sparsity while still displaying exceptional flexibility. This was underscored by the forecasting exercise, where it handily outperformed a static triple gamma prior, as well as the dynamic shrinkage process of [Kowal et al. \(2019\)](#).

Of course, there exist interesting avenues for further research based on the proposed process. As of

now, both  $a_j$  and  $c_j$  are assumed to be fixed for all state variables. Given that it has been shown in the past how shrinkage priors can benefit greatly from sharing information hierarchically (see, for example, [Cadonna et al., 2020](#)), placing hierarchical hyperpriors on these parameters is most likely of interest. Further, [Gourieroux and Jasiak \(2006\)](#) also give blueprints for constructing higher order autoregressive gamma processes, which might increase the flexibility of the dynamic triple gamma even further.

## References

- Belmonte, M., G. Koop, and D. Korobilis (2014). Hierarchical shrinkage in time-varying parameter models. *Journal of Forecasting* 33, 80–94.
- Bhattacharya, A., D. Pati, N. Pillai, and D. B. Dunson (2015). Dirichlet-Laplace priors for optimal shrinkage. *Journal of the American Statistical Association* 110, 1479–1490.
- Bitto, A. and S. Frühwirth-Schnatter (2019). Achieving shrinkage in a time-varying parameter model framework. *Journal of Econometrics* 210, 75–97.
- Cadonna, A., S. Frühwirth-Schnatter, and P. Knaus (2020). Triple the gamma – A unifying shrinkage prior for variance and variable selection in sparse state space and TVP models. *Econometrics* 8, 20.
- Carvalho, C. M., N. G. Polson, and J. G. Scott (2009). Handling sparsity via the horseshoe. *Journal of Machine Learning Research W&CP* 5, 73–80.
- Carvalho, C. M., N. G. Polson, and J. G. Scott (2010). The horseshoe estimator for sparse signals. *Biometrika* 97, 465–480.
- Cobb, G. W. (1978). The problem of the Nile: Conditional solution to a changepoint problem. *Biometrika* 65(2), 243–251.
- Frühwirth-Schnatter, S. (2006). *Finite Mixture and Markov Switching Models*. New York: Springer.
- Frühwirth-Schnatter, S. and H. Wagner (2010). Stochastic model specification search for Gaussian and partially non-Gaussian state space models. *Journal of Econometrics* 154, 85–100.
- George, E. I. and R. McCulloch (1993). Variable selection via Gibbs sampling. *Journal of the American Statistical Association* 88, 881–889.
- George, E. I. and R. McCulloch (1997). Approaches for Bayesian variable selection. *Statistica Sinica* 7, 339–373.
- Gourieroux, C. and J. Jasiak (2006). Autoregressive gamma processes. *Journal of Forecasting* 25, 129–152.
- Griffin, J. E. and P. J. Brown (2010). Inference with normal-gamma prior distributions in regression problems. *Bayesian Analysis* 5, 171–188.
- Griffin, J. E. and P. J. Brown (2017). Hierarchical shrinkage priors for regression models. *Bayesian Analysis* 12, 135–159.
- Hauzenberger, N., F. Huber, G. Koop, and J. Mitchell (2022). Bayesian modeling of time-varying parameters using regression trees. *arXiv preprint arXiv:2209.11970*.
- Hauzenberger, N., F. Huber, G. Koop, and L. Onorante (2021). Fast and flexible bayesian inference in time-varying parameter regression models. *Journal of Business & Economic Statistics*, 1–15.



- Huber, F., G. Kastner, and M. Feldkircher (2019). Should I stay or should I go? A latent threshold approach to large-scale mixture innovation models. *Journal of Applied Econometrics* 34(5), 621–640.
- Huber, F., G. Koop, and L. Onorante (2020). Inducing sparsity and shrinkage in time-varying parameter models. *Journal of Business & Economic Statistics* 0(0), 1–15.
- Huber, F. and M. Pfarrhofer (2021). Dynamic shrinkage in time-varying parameter stochastic volatility in mean models. *Journal of Applied Econometrics* 36(2), 262–270.
- Irie, K. (2019). Bayesian dynamic fused lasso. *arXiv preprint arXiv:1905.12275*.
- Jacquier, E., N. G. Polson, and P. E. Rossi (1994). Bayesian analysis of stochastic volatility models. *Journal of Business & Economic Statistics* 12, 371–417.
- Kalli, M. and J. E. Griffin (2014). Time-varying sparsity in dynamic regression models. *Journal of Econometrics* 178, 779–793.
- Kastner, G. (2016). Dealing with stochastic volatility in time series using the R package stochvol. *Journal of Statistical Software* 69, 1–30.
- Kastner, G. and S. Frühwirth-Schnatter (2014). Ancillarity-sufficiency interweaving strategy (ASIS) for boosting MCMC estimation of stochastic volatility models. *Computational Statistics and Data Analysis* 76, 408–423.
- Knaus, P., A. Bitto-Nemling, A. Cadonna, and S. Frühwirth-Schnatter (2021). Shrinkage in the time-varying parameter model framework using the R package shrinkTVP. *Journal of Statistical Software* 100(13).
- Knaus, P., A. Bitto-Nemling, A. Cadonna, and S. Frühwirth-Schnatter (2022). *shrinkTVP: Efficient Bayesian Inference for Time-Varying Parameter Models with Shrinkage*. R package version 2.0.6.
- Koop, G. and D. Korobilis (2012). Forecasting inflation using dynamic model averaging. *International Economic Review* 53, 867–886.
- Koopman, S. J. and E. Hol Uspensky (2002). The stochastic volatility in mean model: empirical evidence from international stock markets. *Journal of Applied Econometrics* 17(6), 667–689.
- Kowal, D. R., D. S. Matteson, and D. Ruppert (2019). Dynamic shrinkage processes. *Journal of the Royal Statistical Society, Ser. B* 81, 781–804.
- Kraus, E. (1956). Graphs of cumulative residuals. *Quarterly Journal of the Royal Meteorological Society* 82(351), 96–98.
- Lopes, H. F., R. E. McCulloch, and R. S. Tsay (2016). Parsimony inducing priors for large scale state-space models. *Bayesian Analysis*.
- Makalic, E. and D. F. Schmidt (2016). A simple sampler for the horseshoe estimator. *IEEE Signal Processing Letters* 23, 179–182.

- McCausland, W. J., S. Miller, and D. Pelletier (2011). Simulation smoothing for state space models: A computational efficiency analysis. *Computational Statistics and Data Analysis* 55, 199–212.
- Mitchell, T. J. and J. J. Beauchamp (1988). Bayesian variable selection in linear regression. *Journal of the American Statistical Association* 83, 1023–1036.
- Nakajima, J. and M. West (2013). Bayesian dynamic factor models: Latent threshold approach. *Journal of Financial Econometrics* 11, 116–153.
- Park, T. and G. Casella (2008). The Bayesian Lasso. *Journal of the American Statistical Association* 103, 681–686.
- Petris, G. (2010). An R package for Dynamic Linear Models. *Journal of Statistical Software* 36, 1–16.
- Petris, G., S. Petrone, and P. Campagnoli (2009). *Dynamic Linear Models with R*. New York: Springer.
- Polson, N. G. and J. G. Scott (2011). Shrink globally, act locally: Sparse Bayesian regularization and prediction. In J. M. Bernardo, M. J. Bayarri, J. O. Berger, P. Dawid, D. Heckerman, A. F. M. Smith, and M. West (Eds.), *Bayesian Statistics 9*, pp. 501–538. Oxford (UK): Oxford University Press.
- Ročková, V. and K. McAlinn (2021). Dynamic variable selection with spike-and-slab process priors. *Bayesian Analysis* 16(1), 233–269.
- Uribe, P. W. and H. F. Lopes (2020). Dynamic sparsity on dynamic regression models. *arXiv preprint arXiv:2009.14131*.
- van Dyk, D. A. and T. Park (2008). Partially collapsed Gibbs samplers: Theory and methods. *Journal of the American Statistical Association* 103, 790–796.
- Yu, Y. and X.-L. Meng (2011). To center or not to center: that is not the question - an ancillarity-sufficiency interweaving strategy (ASIS) for boosting MCMC efficiency. *Journal of Computational and Graphical Statistics* 20, 531–615.

## Appendix A Details on non-standard distributions

### A.1 The Z-distribution

If  $X \sim Z(\alpha, \beta, \mu_z, \sigma_z)$  follows a Z-distribution, then it has pdf

$$f(x; \alpha, \beta, \mu_z, \sigma_z) = \frac{\exp\left(\frac{z-\mu_z}{\sigma_z}\right)^\alpha \left(1 + \exp\left(\frac{z-\mu_z}{\sigma_z}\right)\right)^{-(\alpha+\beta)}}{\sigma_z B(\alpha, \beta)}. \quad (40)$$

### A.2 The beta-prime distribution

If  $X \sim \mathcal{BP}(a, c)$  follows a beta-prime distribution, then it has pdf

$$f(x; a, c) = \frac{1}{B(a, c)} \frac{x^{a-1}}{(1+x)^{a+c}}.$$

The r.v.  $Y = X/(1+X)$  follows the  $\mathcal{B}(a, c)$ -distribution, meaning that the odds  $X = Y/(1-Y)$  of a  $\mathcal{B}(a, c)$ -distribution follow the  $\mathcal{BP}(a, c)$ -distribution. Furthermore,  $Y = \frac{c}{a}X$  follows the  $F(2a, 2c)$ -distribution. Hence, the beta prime distribution can be represented as the ratio of two independent gamma distributions:

$$\mathcal{BP}(a, c) =_d \frac{\mathcal{G}(a, 1)}{\mathcal{G}(c, 1)}.$$

This follows immediately from

$$\mathcal{BP}(a, c) = \frac{a}{c} F(2a, 2c) =_d \frac{a \mathcal{G}(a, 1) / a}{c \mathcal{G}(c, 1) / c} = \frac{\mathcal{G}(a, 1)}{\mathcal{G}(c, 1)}.$$

## Appendix B Further transition densities of the dynamic triple gamma

### B.1 The transition density $p(\lambda_{jt} | \lambda_{j,t-1}, a_j, c_j, \rho_j)$

The transition density  $\lambda_{jt} | \lambda_{j,t-1}, a_j, c_j, \rho_j$  is marginalized w.r.t.  $\kappa_{jt} | \lambda_{j,t-1}, a_j, c_j, \rho_j$ . The transition density  $\lambda_{jt} | \lambda_{j,t-1}, a_j, c_j, \rho_j$  arises from the rescaled non-central  $\chi^2_{2a_j; \Lambda_{jt}}$ -distribution with  $2a_j$  degrees of freedom and non-centrality parameter

$$\Lambda_{jt} = \frac{2a_j}{c_j} \frac{\rho_j}{1 - \rho_j} \lambda_{j,t-1}. \quad (41)$$

More specifically,

$$p(\lambda_{jt} | \lambda_{j,t-1}, a_j, c_j, \rho_j) = \frac{2a_j}{c_j(1 - \rho_j)} f_{\chi^2_{2a_j; \Lambda_{jt}}} \left( \lambda_{jt} \frac{2a_j}{c_j(1 - \rho_j)} \right), \quad (42)$$

where  $f_{\chi_{2a_j; \Lambda_{jt}}^2}$  is the density of the non-central  $\chi_{2a_j; \Lambda_{jt}}^2$ -distribution.<sup>5</sup> Note that  $\Lambda_{jt}$  is twice the intensity of the Poisson distribution  $\kappa_{jt}|\lambda_{j,t-1}, a_j, c_j, \rho_j$ , while  $\frac{2a_j}{c_j(1-\rho_j)}$  is twice the scale parameter of the gamma distribution  $\lambda_{jt}|\kappa_{jt}, a_j, c_j, \rho_j$ . The proof of (42) is based on rewriting the Gamma density of the r.v.  $\lambda_{jt}|\kappa_{jt}, a_j, c_j, \rho_j$  as

$$\lambda_{jt} = \frac{c_j(1-\rho_j)}{2a_j} X_{jt}, \quad X_{jt}|\kappa_{jt} = k, a_j \sim \mathcal{G}(2(a_j + k)/2, 1/2) \sim \chi_{2a_j+2k}^2.$$

Since  $\kappa_{jt}|\lambda_{j,t-1}, a_j, c_j, \rho_j \sim \mathcal{P}\left(\frac{a_j \rho_j}{c_j(1-\rho_j)} \lambda_{j,t-1}\right) = \mathcal{P}(\Lambda_{jt}/2)$ , it follows immediately that

$$X_{jt}|\lambda_{j,t-1}, a_j, c_j, \rho_j \sim \chi_{2a_j; \Lambda_{jt}}^2$$

follows a non-central  $\chi^2$ -distribution, see also (43). (42) follows immediately from the law of transformation of densities applied to  $X_{jt} = \frac{2a_j}{c_j(1-\rho_j)} \lambda_{jt}$ .

## B.2 The transition density $p(\kappa_{jt}|\kappa_{j,t-1}, a_j, c_j, \rho_j)$

Gourieroux and Jasiak (2006) show that following marginal transition density  $\kappa_{jt}|\kappa_{j,t-1}, a_j, c_j, \rho_j$  holds for  $t = 2, \dots, T$ :

$$\kappa_{jt}|a_j, \rho_j, \kappa_{j,t-1} \sim \text{NegBin}(a_j + \kappa_{j,t-1}, \pi_j), \quad \pi_j = \frac{1}{1 + \rho_j}, \quad (44)$$

while the initial distribution at  $t = 1$  is:

$$\kappa_{j1}|a_j, \rho_j \sim \text{NegBin}(a_j, 1 - \rho_j). \quad (45)$$

This can also be seen directly, as when  $X|Y \sim \mathcal{P}(\vartheta Y)$  and  $Y \sim \mathcal{G}(\alpha, \beta)$ , then  $X \sim \text{NegBin}(\alpha, \pi)$ , where  $\pi = \frac{\beta}{\beta + \vartheta}$ , i.e.

$$\Pr(X = x) = \frac{\Gamma(\alpha + x)}{x! \Gamma(\alpha)} \pi^\alpha (1 - \pi)^x. \quad (46)$$

## B.3 The transition density $p(\kappa_{jt}|\kappa_{j,t-1}, \psi_{j,t-1}, a_j, c_j, \rho_j)$

The transition density (44) is obtained by marginalizing over  $\lambda_{j,t-1}$ . When doing so, one introduces dependence between  $\kappa_{jt}$  and  $\psi_{j,t-1}$  (see also Figure 5). The transition density  $\kappa_{jt}|\kappa_{j,t-1}, \psi_{j,t-1}, \rho_j, a_j, c_j$  is defined as:

$$p(\kappa_{jt}|\kappa_{j,t-1}, \psi_{j,t-1}, a_j, c_j, \rho_j) = \int p(\kappa_{jt}|\lambda_{j,t-1}, a_j, c_j, \rho_j) p(\lambda_{j,t-1}|\kappa_{j,t-1}, \psi_{j,t-1}, a_j, c_j, \rho_j) d\lambda_{j,t-1}.$$

<sup>5</sup>The noncentral chi-squared distribution,  $Y \sim \chi_{\nu; \Lambda}^2$  can be seen as a Poisson-weighted mixture of central chi-squared distributions:

$$f_{\chi_{\nu; \Lambda}^2}(y) = \sum_{k=0}^{\infty} \frac{e^{-\Lambda/2} (\Lambda/2)^k}{k!} f_{\chi_{\nu+2k}^2}(y), \quad (43)$$

where  $f_{\chi_{\nu+2k}^2}(y)$  is the density of a  $\chi_{\nu+2k}^2$ -distribution.

Using<sup>6</sup>

$$\lambda_{j,t-1}|\kappa_{j,t-1}, \psi_{j,t-1}, a_j, c_j, \rho_j \sim \mathcal{G}\left(a_j + c_j + \kappa_{j,t-1}, \frac{a_j}{c_j} \frac{1}{1-\rho_j} + \frac{1}{\psi_{j,t-1}}\right), \quad (47)$$

in combination with (46), we obtain following negative binomial distribution:

$$\begin{aligned} \kappa_{jt}|\kappa_{j,t-1}, \psi_{j,t-1}, \rho_j, a_j, c_j &\sim \text{NegBin}(a_j + c_j + \kappa_{j,t-1}, \pi_{j,t-1}), \\ \pi_{j,t-1} &= \frac{a_j \psi_{j,t-1} + c_j(1-\rho_j)}{(1+\rho_j)a_j \psi_{j,t-1} + c_j(1-\rho_j)}. \end{aligned} \quad (48)$$

In comparison to the transition density (44), we find that  $c_j$  adds to the “number of trials” (the first parameter), while the “success probability”  $\pi_{j,t-1}$  (the second parameter) is time-varying and depends on the past scale  $\psi_{j,t-1}$ , as opposed to the fixed success probability  $\pi_j$  in (44). For  $\rho_j = 1$  and  $\psi_{j,t-1} = \infty$ , the two probabilities coincide,  $\pi_{j,t-1} = \pi_j$ , otherwise  $\psi_{j,t-1}$  will impact  $\pi_{j,t-1}$ .

#### B.4 The transition density $p(\psi_{jt}|\kappa_{jt}, a_j, c_j, \rho_j)$

Combining representation (12) with the conditional density  $\lambda_{jt}|\kappa_{jt}, a_j, c_j, \rho_j \sim \mathcal{G}\left(a_j + \kappa_{jt}, \frac{a_j}{c_j} \frac{1}{1-\rho_j}\right)$ , it is possible to derive the following closed form representation of  $p(\psi_{jt}|\kappa_{jt}, a_j, c_j, \rho_j)$ :

$$p(\psi_{jt}|\kappa_{jt}, a_j, c_j, \rho_j) = \frac{1}{B(a_j + \kappa_{jt}, c_j)} \frac{a_j}{c_j(1-\rho_j)} \left(\frac{a_j \psi_{jt}}{c_j(1-\rho_j)}\right)^{a_j + \kappa_{jt} - 1} \left(\frac{a_j \psi_{jt}}{c_j(1-\rho_j)} + 1\right)^{-(a_j + c_j + \kappa_{jt})}. \quad (49)$$

This implies that  $\psi_{jt}|\kappa_{jt}, a_j, c_j, \rho_j \sim \mathcal{BP}\left(a_j + \kappa_{jt}, c_j, 1, \frac{c_j(1-\rho_j)}{a_j}\right)$ , where  $\mathcal{BP}(\alpha, \beta, p, q)$  is the generalized beta prime distribution.

*Proof of (49).*

$$\begin{aligned} p(\psi_{jt}|\kappa_{jt}, a_j, c_j, \rho_j) &= \int p(\psi_{jt}|\kappa_{jt}, \lambda_{jt}, a_j, c_j, \rho_j) p(\lambda_{jt}|\kappa_{jt}, a_j, c_j, \rho_j) d\lambda_{jt} = \\ &= \frac{1}{\Gamma(c_j)\Gamma(a_j + \kappa_{jt})} \left(\frac{1}{\psi_{jt}}\right)^{c_j+1} \left(\frac{a_j}{c_j(1-\rho_j)}\right)^{a_j + \kappa_{jt}} \\ &\quad \cdot \int \lambda_{jt}^{c_j} \exp\left(-\frac{\lambda_{jt}}{\psi_{jt}}\right) \lambda_{jt}^{a_j + \kappa_{jt} - 1} \exp\left(-\frac{\lambda_{jt} a_j}{c_j(1-\rho_j)}\right) d\lambda_{jt} = \\ &= \frac{\Gamma(a_j + c_j + \kappa_{jt})}{\Gamma(c_j)\Gamma(a_j + \kappa_{jt})} \left(\frac{1}{\psi_{jt}}\right)^{c_j+1} \left(\frac{a_j}{c_j(1-\rho_j)}\right)^{a_j + \kappa_{jt}} \left(\frac{a_j}{c_j(1-\rho_j)} + \frac{1}{\psi_{jt}}\right)^{-(a_j + c_j + \kappa_{jt})} = \\ &= \frac{1}{B(a_j + \kappa_{jt}, c_j)} \frac{a_j}{c_j(1-\rho_j)} \left(\frac{a_j \psi_{jt}}{c_j(1-\rho_j)}\right)^{a_j + \kappa_{jt} - 1} \left(\frac{a_j \psi_{jt}}{c_j(1-\rho_j)} + 1\right)^{-(a_j + c_j + \kappa_{jt})}. \end{aligned}$$

(49) together with (48) and (45) defines a new state space model with the same properties as the one introduced in Section 2, albeit with less convenient conditional densities involved. A representation of this new state space model as a directed graph can be found in Figure 5.

<sup>6</sup>Same derivation as for  $\lambda_{jT}|\kappa_{jT}, \psi_{jT}, a_j, c_j, \rho_j$  in full conditional Gibbs, see Appendix D.1

## B.5 The transition density $p(\psi_{jt}|\lambda_{j,t-1}, a_j, c_j, \rho_j)$

The transition density  $\psi_{jt}|\lambda_{j,t-1}, a_j, c_j, \rho_j$  is marginalized w.r.t.  $\kappa_{jt}|\lambda_{j,t-1}, a_j, c_j, \rho_j$ . The transition density  $\psi_{jt}|\lambda_{j,t-1}, a_j, c_j, \rho_j$  arises from the rescaled non-central F  $(2a_j, 2c_j; \Lambda_{jt})$ -distribution with  $2a_j$  and  $2c_j$  degrees of freedom respectively, and the same non-centrality parameter  $\Lambda_{jt}$  defined in (42). More specifically,

$$p(\psi_{jt}|\lambda_{j,t-1}, a_j, c_j, \rho_j) = \frac{1}{1 - \rho_j} f_{\mathbf{F}(2a_j, 2c_j; \Lambda_{jt})} \left( \frac{\psi_{jt}}{1 - \rho_j} \right), \quad (50)$$

where  $f_{\mathbf{F}(2a_j, 2c_j; \Lambda_{jt})}$  is the density of the non-central F  $(2a_j, 2c_j; \Lambda_{jt})$ -distribution.<sup>7</sup>

The proof of (50) is based on rewriting the density of the r.v.  $\psi_{jt}|\kappa_{jt}, a_j, c_j, \rho_j$  as

$$\psi_{jt} = (1 - \rho_j)X_{jt}, \quad X_{jt}|\kappa_{jt} = k, a_j, c_j \sim \mathbf{F}(2(a_j + k), 2c_j).$$

This representations follows immediately from the density of an F-distribution and (49). Since  $\kappa_{jt}|\lambda_{j,t-1}, a_j, c_j, \rho_j \sim \mathcal{P}(\Lambda_{jt}/2)$ , it follows immediately that

$$X_{jt}|\lambda_{j,t-1}, a_j, c_j, \rho_j \sim \mathbf{F}(2a_j, 2c_j; \Lambda_{jt})$$

follows a non-central F-distribution, see also (51). (50) follows immediately from the law of transformation of densities applied to  $X_{jt} = \frac{\psi_{jt}}{1 - \rho_j}$ .

## Appendix C Proofs

*Proof of Theorem 1:* The proof is based on combining (50) with the density  $p(\lambda_{jt}|\psi_{jt}, a_j, c_j)$ , the latter of which can be easily derived under the assumption that  $\lambda_{jt} \sim \mathcal{G}\left(a_j, \frac{a_j}{c_j}\right)$  via Bayes theorem. To this end, note that

$$\begin{aligned} p(\lambda_{jt}|\psi_{jt}, a_j, c_j) &\propto p(\psi_{jt}|\lambda_{jt}, a_j, c_j)p(\lambda_{jt}|a_j, c_j) \\ &\propto \lambda_{jt}^{c_j} e^{-\lambda_{jt} \frac{1}{\psi_{jt}}} \lambda_{jt}^{a_j-1} e^{-\lambda_{jt} \frac{a_j}{c_j}} \\ &= \lambda_{jt}^{a_j+c_j-1} e^{-\lambda_{jt} \left( \frac{1}{\psi_{jt}} + \frac{a_j}{c_j} \right)}, \end{aligned}$$

from which it follows that

$$\lambda_{jt}|\psi_{jt}, a_j, c_j \sim \mathcal{G}\left(a_j + c_j, \frac{1}{\psi_{jt}} + \frac{a_j}{c_j}\right). \quad (52)$$

Taking this, combining it with (50) and letting

$$A = \frac{1}{1 - \rho_j} \frac{\left( \frac{1}{\psi_{j,t-1}} + \frac{a_j}{c_j} \right)^{a_j+c_j}}{\Gamma(a_j + c_j)}$$

<sup>7</sup>The noncentral F-distribution,  $Y \sim \mathbf{F}(\nu_1, \nu_2; \Lambda)$ , has the density function

$$f_{\mathbf{F}(\nu_1, \nu_2; \Lambda)}(y) = \sum_{k=0}^{\infty} \frac{e^{-\Lambda/2} (\Lambda/2)^k}{B\left(\frac{\nu_2}{2}, \frac{\nu_1}{2} + k\right) k!} \left(\frac{\nu_1}{\nu_2}\right)^{\frac{\nu_1}{2}+k} \left(\frac{\nu_2}{\nu_2 + \nu_1 y}\right)^{\frac{\nu_1+\nu_2}{2}+k} y^{\nu_1/2-1+k}. \quad (51)$$

and

$$C(k) = \frac{\left(\frac{a_j \rho_j}{c_j(1-\rho_j)}\right)^k \left(\frac{a_j}{c_j}\right)^{a_j+k} \left(\frac{c_j}{c_j + \frac{a_j \psi_{jt}}{1-\rho_j}}\right)^{a_j+c_j+k} \left(\frac{\psi_{jt}}{1-\rho_j}\right)^{a_j+k-1}}{B(a_j + k, c_j)}$$

yields

$$\begin{aligned} p(\psi_{jt}|\psi_{j,t-1}, a_j, c_j, \rho_j) &= \int_0^\infty p(\psi_{jt}|\lambda_{j,t-1}, a_j, c_j, \rho_j)p(\lambda_{j,t-1}|\psi_{j,t-1}, a_j, c_j)d\lambda_{j,t-1} \\ &= A \int_0^\infty \left[ \sum_{k=0}^\infty C(k) e^{-\frac{a_j}{c_j} \frac{\rho_j}{1-\rho_j} \lambda_{j,t-1}} \lambda_{j,t-1}^k \right] \lambda_{j,t-1}^{a_j+c_j-1} e^{-\lambda_{j,t-1} \left( \frac{1}{\psi_{j,t-1}} + \frac{a_j}{c_j} \right)} d\lambda_{j,t-1} \\ &= A \sum_{k=0}^\infty C(k) \int_0^\infty \lambda_{j,t-1}^{a_j+c_j+k-1} e^{-\left( \frac{a_j}{c_j} \frac{1}{1-\rho_j} + \frac{1}{\psi_{j,t-1}} \right) \lambda_{j,t-1}} d\lambda_{j,t-1} \\ &= A \sum_{k=0}^\infty C(k) \frac{\Gamma(a_j + c_j + k)}{\left( \frac{a_j}{c_j} \frac{1}{1-\rho_j} + \frac{1}{\psi_{j,t-1}} \right)^{a_j+c_j+k}}. \end{aligned}$$

Combined with the definition of the hypergeometric function and after some algebraic manipulations the above results in (15).

*Proof of Theorem 2:* The derivation of this result relies on the tower property combined with (50) and  $p(\lambda_{j,t-1}|\psi_{j,t-1}, a_j, c_j)$ . First, note that

$$\mathbb{E}[\psi_{jt}|\psi_{j,t-1}, a_j, c_j, \rho_j] = \mathbb{E}[\mathbb{E}[\psi_{jt}|\lambda_{j,t-1}, a_j, c_j]|\psi_{j,t-1}, a_j, c_j, \rho_j].$$

Based on (50) and the properties of the noncentral F-distribution (which requires that  $c_j > 1$  for the expected value to exist), it can be deduced that

$$\begin{aligned} \mathbb{E}[\psi_{jt}|\lambda_{j,t-1}, a_j, c_j] &= (1 - \rho_j) \mathbb{E} \left[ \frac{\psi_{jt}}{(1 - \rho_j)} | \lambda_{j,t-1}, a_j, c_j \right] \\ &= (1 - \rho_j) \frac{c_j}{c_j - 1} + \rho_j \frac{1}{c_j - 1} \mathbb{E}[\lambda_{j,t-1} | \psi_{j,t-1}, a_j, c_j], \end{aligned}$$

which, through the use of the properties of the gamma distribution leads to

$$\mathbb{E}[\psi_{jt}|\lambda_{j,t-1}, a_j, c_j] = (1 - \rho_j) \frac{c_j}{c_j - 1} + \rho_j \frac{1}{c_j - 1} \frac{a_j + c_j}{\frac{1}{\psi_{j,t-1}} + \frac{a_j}{c_j}}.$$

Following some algebraic manipulations, this results in (18).



## Appendix D Details on the MCMC scheme

### D.1 Full conditional Gibbs sampling for all variables

Full conditional Gibbs sampling operates in the original state space representation of model depicted in Figure 2. This MCMC sampler loops over the coefficients for  $j = 1, \dots, d$  to sample the latent variables  $\lambda_{j0}, \{\psi_{jt}, \lambda_{jt}, \kappa_{jt}\}_{t=1}^T | \{\tilde{\beta}_{jt}\}_{t=0}^T, a_j, c_j, \rho_j, \theta_j$  as well as the coefficient  $\rho_j | \{\psi_{jt}, \lambda_{jt}, \kappa_{jt}\}_{t=1}^T, \lambda_{j0}, \{\tilde{\beta}_{jt}\}_{t=0}^T, a_j, c_j$ :

(a) For  $1 \leq t \leq T$ , sample  $\kappa_{jt} | \lambda_{jt}, \lambda_{j,t-1}, a_j, c_j, \rho_j$  from the discrete distribution given in (33).

(b) Using (30) for  $1 \leq t \leq T$ , sample

$$\psi_{jt} | w_{jt}, \lambda_{jt}, \theta_j, c_j \sim \mathcal{G}^{-1} \left( c_j + \frac{1}{2}, \frac{w_{jt}^2}{2\theta_j} + \lambda_{jt} \right).$$

(c) For  $1 \leq t \leq T - 1$ , sample

$$\lambda_{jt} | \psi_{jt}, \kappa_{jt}, \kappa_{j,t+1}, a_j, c_j, \rho_j \sim \mathcal{G} \left( a_j + c_j + \kappa_{jt} + \kappa_{j,t+1}, \frac{a_j}{c_j} \frac{1 + \rho_j}{1 - \rho_j} + \frac{1}{\psi_{jt}} \right),$$

see (32); sample  $\lambda_{j0} | \kappa_{j1}, a_j, c_j, \rho_j$  and  $\lambda_{jT} | \psi_{jT}, \kappa_{jT}, a_j, c_j, \rho_j$  as in (53) and (54), respectively.

(d) Sample  $\rho_j | \{\lambda_{jt}, \kappa_{jt}\}_{t=1}^T, \lambda_{j0}, a_j, c_j$  using an MH-step.

Modifications are needed for sampling  $\lambda_{jt}$  when  $t = 0$  and  $t = T$ , namely:

$$\lambda_{j0} | \kappa_{j1}, a_j, c_j, \rho_j \sim \mathcal{G} \left( a_j + \kappa_{j1}, \frac{a_j}{c_j} \frac{1}{1 - \rho_j} \right), \quad (53)$$

and

$$\lambda_{jT} | \psi_{jT}, \kappa_{jT}, a_j, c_j, \rho_j \sim \mathcal{G} \left( a_j + c_j + \kappa_{jT}, \frac{a_j}{c_j} \frac{1}{1 - \rho_j} + \frac{1}{\psi_{jT}} \right). \quad (54)$$

Note that the sampling order is arbitrary in this sampler.

## D.2 Marginalized Gibbs sampler

To simplify notation in Algorithm 1, let  $\mathbf{y} = (y_1, \dots, y_T)$  denote the observed time series,  $\mathbf{X} = (\mathbf{x}_1, \dots, \mathbf{x}_T)$  represent the observed regressors, and  $\mathbf{z}$  be the set of all latent variables and unknown model parameters in a TVP model with time-varying innovation variances. This allows us to define  $\mathbf{z}_{-x}$  as the set of all unknowns aside from  $x$ .

---

**Algorithm 1.** *MCMC inference for TVP models under the dynamic triple gamma prior.*

---

Choose starting values for all parameters except  $\beta_0, \dots, \beta_T, \rho_1, \dots, \rho_d$  and repeat the following steps:

- (a) Sample  $\beta_0, \dots, \beta_T, \beta_1, \dots, \beta_d, \theta_1, \dots, \theta_d | \psi_1, \dots, \psi_T, \sigma_1^2, \dots, \sigma_T^2, \mathbf{y}, \mathbf{X}$  and all associated hyperparameters using Algorithm 1, steps (a) - (d) in Cadonna et al. (2020).
- (b) (b.1) In the homoscedastic case, sample  $\sigma^2 | \mathbf{z}_{-\sigma^2}, \mathbf{y}, \mathbf{X}$  using Algorithm 1, step (f) in Bitto and Frühwirth-Schnatter (2019).
- (b.2) In the SV case defined in (3), sample  $\sigma_1^2, \dots, \sigma_T^2, \sigma_\eta^2, \mu, \phi | \mathbf{z}_{-\sigma^2}, \mathbf{y}, \mathbf{X}$  as in Kastner and Frühwirth-Schnatter (2014), for example via the R-package `stochvol` (Kastner, 2016).
- (c) For  $j = 1, \dots, d$ , perform the following sampling steps:
  - (1) Use the approximate prior  $p(\psi_{jt} | \psi_{j,t-1}, a_j, c_j, \rho_j)$  marginalized w.r.t.  $\lambda_{j1}, \dots, \lambda_{j,t-1}$  and  $\kappa_{j1}, \dots, \kappa_{j,t-1}$  to construct the approximate conditional likelihood

$$p(\psi_{j1}, \dots, \psi_{jT} | a_j, c_j, \rho_j) \approx \prod_{t=1}^T p(\psi_{jt} | \psi_{j,t-1}, a_j, c_j, \rho_j) = f(\psi_{j1}, \dots, \psi_{jT} | a_j, c_j, \rho_j),$$

to sample  $\rho_j$  via a random walk MH step on  $z = \log(\rho_j / (b_\rho - \rho_j))$ . Propose  $\rho_j^* = b_\rho e^{z^*} / (1 + e^{z^*})$ , where  $z^* \sim \mathcal{N}(z^{(m-1)}, v^2)$  and  $z^{(m-1)} = \log(\rho_j^{(m-1)} / (b_\rho - \rho_j^{(m-1)}))$  depends on the previously sampled value  $\rho_j^{(m-1)}$  of  $\rho_j$ . Accept  $\rho_j^*$  with probability

$$\min \left\{ 1, \frac{q_\rho(\rho_j^*)}{q_\rho(\rho_j^{(m-1)})} \right\}, \quad q_\rho(\rho_j) = f(\psi_{j1}, \dots, \psi_{jT} | a_j, c_j, \rho_j) p(\rho_j) \rho_j (b_\rho - \rho_j).$$

- (2) For  $t = 2, \dots, T - 1$ , sample  $\kappa_{jt}$  from the following discrete distribution marginalized w.r.t.  $\lambda_{j1}, \dots, \lambda_{jT}$ :

$$p(\kappa_{jt} | \kappa_{j,t-1}, \kappa_{j,t+1}, \psi_{jt}, \psi_{j,t-1}, \rho_j, a_j, c_j) \propto \frac{\Gamma(a_j + c_j + \kappa_{j,t-1} + \kappa_{jt}) \Gamma(a_j + c_j + \kappa_{jt} + \kappa_{j,t+1})}{\kappa_{jt}! \Gamma(a_j + \kappa_{jt})} \left[ (1 - \pi_{j,t-1}) \pi_{jt} \frac{a_j \psi_{jt}}{a_j \psi_{jt} + c_j (1 - \rho_j)} \right]^{\kappa_{jt}}.$$

Further, sample  $\kappa_{j1}$  from

$$p(\kappa_{j1} | \kappa_{j2}, \psi_{j1}, \rho_j, a_j, c_j) \propto \frac{\Gamma(a_j + c_j + \kappa_{j1} + \kappa_{j2}) \Gamma(a_j + \kappa_{j1})}{\Gamma(a_j + \kappa_{j1}) \kappa_{j1}!} \left[ \rho_j \pi_{j1} \frac{a_j \psi_{j1}}{a_j \psi_{j1} + c_j (1 - \rho_j)} \right]^{\kappa_{j1}},$$

and  $\kappa_{jT}$  from

$$p(\kappa_{jT}|\kappa_{j,T-1}, \psi_{j,T-1}, \psi_{jT}, \rho_j, a_j, c_j) \\ \propto \frac{\Gamma(a_j + c_j + \kappa_{j,T-1} + \kappa_{jT})\Gamma(a_j + c_j + \kappa_{jT})}{\Gamma(a_j + \kappa_{jT})\kappa_{jT}!} \left[ (1 - \pi_{j,T-1}) \frac{a_j \psi_{jT}}{a_j \psi_{jT} + c_j(1 - \rho_j)} \right]^{\kappa_{jT}}.$$

Efficient sampling from these densities is discussed in Section D.2.1.

- (3) For  $t = 1, \dots, T - 1$ , sample  $\lambda_{jt}$  from a gamma distribution

$$\lambda_{jt}|\psi_{jt}, \kappa_{jt}, \kappa_{j,t+1}, a_j, c_j, \rho_j \sim \mathcal{G} \left( a_j + c_j + \kappa_{jt} + \kappa_{j,t+1}, \frac{a_j}{c_j} \frac{1 + \rho_j}{1 - \rho_j} + \frac{1}{\psi_{jt}} \right).$$

Further, for  $t = 0$ , sample  $\lambda_{j0}$  from

$$\lambda_{j0}|\kappa_{j1}, a_j, c_j, \rho_j \sim \mathcal{G} \left( a_j + \kappa_{j1}, \frac{a_j}{c_j} \frac{1}{1 - \rho_j} \right),$$

and  $\lambda_{jT}$  from

$$\lambda_{jT}|\psi_{jT}, \kappa_{jT}, a_j, c_j, \rho_j \sim \mathcal{G} \left( a_j + c_j + \kappa_{jT}, \frac{a_j}{c_j} \frac{1}{1 - \rho_j} + \frac{1}{\psi_{jT}} \right).$$

- (4) For  $t = 1, \dots, T$  sample  $\psi_{jt}$  from an inverse gamma distribution

$$\psi_{jt}|w_{jt}, \lambda_{jt}, c_j \sim \mathcal{G}^{-1} \left( c_j + \frac{1}{2}, \lambda_{jt} + \frac{w_{jt}^2}{2\theta_j} \right).$$

In step (c)(1) of Algorithm 1,

$$q_\rho(\rho_j) = f(\psi_{j1}, \dots, \psi_{jT}|a_j, c_j, \rho_j) p(\rho_j) \rho_j (b_\rho - \rho_j) \\ \propto \left[ \prod_{t=1}^T {}_2F_1 \left( a_j + c_j, a_j + c_j, a_j, \frac{a_j^2 \rho_j \psi_{jt} \psi_{j,t-1}}{(a_j \psi_{jt} + c_j(1 - \rho_j))(a_j \psi_{j,t-1} + c_j(1 - \rho_j))} \right) \right. \\ \left. \times \left( \frac{(1 - \rho_j)}{\left( c_j + \frac{a_j \psi_{jt}}{1 - \rho_j} \right) (a_j \psi_{j,t-1} + c_j(1 - \rho_j))} \right)^{a_j + c_j} \right] (1 - \rho_j)^{-T a_j} \\ \times \rho_j^{a_\rho \alpha_\rho - 1} (1 - (\rho_j/b_\rho)^{a_\rho})^{\beta_\rho - 1} \rho_j (b_\rho - \rho_j).$$

Hence,  $\log q_\rho(\rho_j)$  is given by

$$\log q_\rho(\rho_j) = \left[ \sum_{t=1}^T \log {}_2F_1 \left( a_j + c_j, a_j + c_j, a_j, \frac{a_j^2 \rho_j \psi_{jt} \psi_{j,t-1}}{(a_j \psi_{jt} + c_j(1 - \rho_j))(a_j \psi_{j,t-1} + c_j(1 - \rho_j))} \right) \right. \\ \left. + (a_j + c_j) \left( \log(1 - \rho_j) - \log \left( c_j + \frac{a_j \psi_{jt}}{1 - \rho_j} \right) - \log(a_j \psi_{j,t-1} + c_j(1 - \rho_j)) \right) \right] \\ - T a_j \log(1 - \rho_j) + (a_\rho \alpha_\rho - 1) \log \rho_j + (\beta_\rho - 1) \log(1 - (\rho_j/b_\rho)^{a_\rho}) \\ + \log \rho_j + \log(b_\rho - \rho_j).$$

For step (c)(2), it is important to note that the approximate conditional likelihood in (c)(1) is marginalized w.r.t.  $\lambda_{j1}, \dots, \lambda_{jT}$  and  $\kappa_{j1}, \dots, \kappa_{jT}$ . Therefore, to preserve the stationary distribution of the Markov chain, one needs to sample  $\kappa_{j1}, \dots, \kappa_{jT}$  from a density that is marginalized w.r.t.  $\lambda_{j1}, \dots, \lambda_{jT}$ . As such, one has to turn to the alternate state space representation in defined by (49) together with (48) and (45) and visualized in Figure 5. Hence, the posterior  $\kappa_{jt}|\kappa_{j,t-1}, \kappa_{j,t+1}, \psi_{jt}, \psi_{j,t-1}, \rho_j, a_j, c_j$  is given by:

$$p(\kappa_{jt}|\kappa_{j,t-1}, \kappa_{j,t+1}, \psi_{jt}, \psi_{j,t-1}, \rho_j, a_j, c_j) \propto p(\kappa_{jt}|\kappa_{j,t-1}, \psi_{j,t-1}, a_j, c_j, \rho_j)p(\kappa_{j,t+1}|\kappa_{jt}, \psi_{jt}, a_j, c_j, \rho_j)p(\psi_{jt}|\kappa_{jt}, a_j, c_j, \rho_j).$$

Both transition densities  $p(\kappa_{jt}|\kappa_{j,t-1}, \psi_{j,t-1}, a_j, c_j, \rho_j)$  and  $p(\kappa_{j,t+1}|\kappa_{jt}, \psi_{jt}, a_j, c_j, \rho_j)$  are equal to the negative binomial transition density derived in (48), i.e.

$$p(\kappa_{jt}|\kappa_{j,t-1}, \psi_{j,t-1}, \rho_j, a_j, c_j) = \frac{\Gamma(a_j + c_j + \kappa_{j,t-1} + \kappa_{jt})}{\kappa_{jt}!\Gamma(a_j + c_j + \kappa_{j,t-1})} (\pi_{j,t-1})^{a_j + c_j + \kappa_{j,t-1}} (1 - \pi_{j,t-1})^{\kappa_{jt}},$$

$$p(\kappa_{j,t+1}|\kappa_{jt}, \psi_{jt}, \rho_j, a_j, c_j) = \frac{\Gamma(a_j + c_j + \kappa_{jt} + \kappa_{j,t+1})}{\kappa_{j,t+1}!\Gamma(a_j + c_j + \kappa_{jt})} (\pi_{jt})^{a_j + c_j + \kappa_{jt}} (1 - \pi_{jt})^{\kappa_{j,t+1}}.$$

while  $p(\psi_{jt}|\kappa_{jt}, a_j, c_j, \rho_j)$  arises from the rescaled beta prime distribution derived in (49):

$$p(\psi_{jt}|\kappa_{jt}, a_j, c_j, \rho_j) = \frac{1}{B(a_j + \kappa_{jt}, c_j)} \frac{a_j}{c_j(1 - \rho_j)} \left( \frac{a_j \psi_{jt}}{c_j(1 - \rho_j)} \right)^{a_j + \kappa_{jt} - 1} \left( \frac{a_j \psi_{jt}}{c_j(1 - \rho_j)} + 1 \right)^{-(a_j + c_j + \kappa_{jt})}.$$

This yields:

$$\begin{aligned} & p(\kappa_{jt}|\kappa_{j,t-1}, \kappa_{j,t+1}, \psi_{jt}, \psi_{j,t-1}, \rho_j, a_j, c_j) \tag{55} \\ \propto & \frac{\Gamma(a_j + c_j + \kappa_{j,t-1} + \kappa_{jt})}{\kappa_{jt}!\Gamma(a_j + c_j + \kappa_{j,t-1})} (\pi_{j,t-1})^{a_j + c_j + \kappa_{j,t-1}} (1 - \pi_{j,t-1})^{\kappa_{jt}} \\ & \cdot \frac{\Gamma(a_j + c_j + \kappa_{jt} + \kappa_{j,t+1})}{\kappa_{j,t+1}!\Gamma(a_j + c_j + \kappa_{jt})} (\pi_{jt})^{a_j + c_j + \kappa_{jt}} (1 - \pi_{jt})^{\kappa_{j,t+1}} \\ & \cdot \frac{1}{B(a_j + \kappa_{jt}, c_j)} \frac{a_j}{c_j(1 - \rho_j)} \left( \frac{a_j \psi_{jt}}{c_j(1 - \rho_j)} \right)^{a_j + \kappa_{jt} - 1} \left( \frac{a_j \psi_{jt}}{c_j(1 - \rho_j)} + 1 \right)^{-(a_j + c_j + \kappa_{jt})} \\ \propto & \frac{\Gamma(a_j + c_j + \kappa_{j,t-1} + \kappa_{jt})\Gamma(a_j + c_j + \kappa_{jt} + \kappa_{j,t+1})}{\kappa_{jt}!\Gamma(a_j + \kappa_{jt})} \left[ (1 - \pi_{j,t-1})\pi_{jt} \frac{a_j \psi_{jt}}{a_j \psi_{jt} + c_j(1 - \rho_j)} \right]^{\kappa_{jt}}. \end{aligned}$$

Modifications are needed for  $t = 1$  and  $t = T$ . For  $t = 1$ , the prior  $p(\kappa_{j1}|a_j, c_j, \rho_j)$  is equal to the stationary distribution  $\kappa_{j1}|a_j, \rho_j \sim \text{NegBin}(a_j, 1 - \rho_j)$  given in (45) and is combined with the likelihoods  $p(\kappa_{j2}|\kappa_{j1}, \psi_{j1}, a_j, c_j, \rho_j)$  and  $p(\psi_{jT}|\kappa_{jT}, a_j, c_j, \rho_j)$ :

$$p(\kappa_{j1}|\kappa_{j2}, \psi_{j1}, \rho_j, a_j, c_j) \propto p(\kappa_{j2}|\kappa_{j1}, \psi_{j1}, a_j, c_j, \rho_j)p(\kappa_{j1}|a_j, \rho_j) \propto \frac{\Gamma(a_j + c_j + \kappa_{j1} + \kappa_{j2})\Gamma(a_j + \kappa_{j1})}{\Gamma(a_j + \kappa_{j1})\kappa_{j1}!} \left[ \rho_j \pi_{j1} \frac{a_j \psi_{j1}}{a_j \psi_{j1} + c_j(1 - \rho_j)} \right]^{\kappa_{j1}}. \tag{56}$$

For  $t = T$ , the prior  $p(\kappa_{jT}|\kappa_{j,T-1}, \psi_{j,T-1}, a_j, c_j, \rho_j)$  is combined with the likelihood  $p(\psi_{jT}|\kappa_{jT}, a_j, c_j, \rho_j)$ :

$$p(\kappa_{jT}|\kappa_{j,T-1}, \psi_{j,T-1}, \psi_{jT}, \rho_j, a_j, c_j) \propto p(\kappa_{jT}|\kappa_{j,T-1}, \psi_{j,T-1}, \rho_j, a_j, c_j)p(\psi_{jT}|\kappa_{jT}, a_j, c_j, \rho_j) \propto \frac{\Gamma(a_j + c_j + \kappa_{j,T-1} + \kappa_{jT})\Gamma(a_j + c_j + \kappa_{jT})}{\Gamma(a_j + \kappa_{jT})\kappa_{jT}!} \left[ (1 - \pi_{j,T-1}) \frac{a_j \psi_{jT}}{a_j \psi_{jT} + c_j(1 - \rho_j)} \right]^{\kappa_{jT}} \tag{57}$$

	$t = 1$	$t = 2, \dots, T - 1$	$t = T$
$a_{jt}^\kappa$	$a_j$	$a_j + c_j + \kappa_{j,t-1}$	$a_j + c_j + \kappa_{j,T-1}$
$b_{jt}^\kappa$	$a_j + c_j + \kappa_{j2}$	$a_j + c_j + \kappa_{j,t+1}$	$a_j + c_j$
$c_j^\kappa$	$a_j$	$a_j$	$a_j$
$z_{jt}^\psi$	$\frac{\rho_j \pi_{j1} a_j \psi_{j1}}{a_j \psi_{j1} + c_j (1 - \rho_j)}$	$\frac{(1 - \pi_{j,t-1}) \pi_{jt} a_j \psi_{jt}}{a_j \psi_{jt} + c_j (1 - \rho_j)}$	$\frac{(1 - \pi_{j,T-1}) a_j \psi_{jT}}{a_j \psi_{jT} + c_j (1 - \rho_j)}$

Table 1: Constants required for the derivation of the function  ${}_2F_1(a_{jt}^\kappa, b_{jt}^\kappa; c_j^\kappa; z_{jt}^\psi)$  for the normalising constant of  $\kappa_{jt} | \kappa_{j,t-1}, \kappa_{j,t+1}, \psi_{jt}, \psi_{j,t-1}, \rho_j, a_j, c_j$ . Note that  $\pi_{jt} = \frac{a_j \psi_{jt} + c_j (1 - \rho_j)}{(1 + \rho_j) a_j \psi_{jt} + c_j (1 - \rho_j)}$ , as in (48).

Hence, the posterior  $p(\kappa_{jt} | \kappa_{j,s}, \psi_{j,r}, \rho_j, a_j, c_j)$ , where  $s \in \{\max(t - 1, 1), \min(t + 1, T)\}$  and  $r \in \{\max(t - 1, 1), t\}$  is proportional to

$$p(\kappa_{jt} | \kappa_{j,s}, \psi_{j,r}, \rho_j, a_j, c_j) \propto \frac{\Gamma(a_{jt}^\kappa + \kappa_{jt}) \Gamma(b_{jt}^\kappa + \kappa_{jt}) (z_{jt}^\psi)^{\kappa_{jt}}}{\Gamma(c_j^\kappa + \kappa_{jt}) \kappa_{jt}!}, \quad (58)$$

for  $t = 1, \dots, T$ , where  $a_{jt}^\kappa, b_{jt}^\kappa, c_j^\kappa$  and  $z_{jt}^\psi$  are defined in Table 1. It follows immediately from the definition of the hypergeometric presented in (16) and (17) that the normalizing constant of this density can be expressed with the help of the hypergeometric function, for all  $t = 1, \dots, T$ :

$$\sum_{\kappa_{jt}=0}^{\infty} \frac{\Gamma(a_{jt}^\kappa + \kappa_{jt}) \Gamma(b_{jt}^\kappa + \kappa_{jt}) (z_{jt}^\psi)^{\kappa_{jt}}}{\Gamma(c_j^\kappa + \kappa_{jt}) \kappa_{jt}!} = \frac{\Gamma(a_{jt}^\kappa) \Gamma(b_{jt}^\kappa)}{\Gamma(c_j^\kappa)} {}_2F_1(a_{jt}^\kappa, b_{jt}^\kappa; c_j^\kappa; z_{jt}^\psi), \quad (59)$$

This allows for very efficient sampling from these densities, see Section D.2.1.

Step (c)(3) is more straightforward, as we can simply sample from the full conditional distribution again. For  $t = 1, \dots, T - 1$ :

$$\begin{aligned} p(\lambda_{jt} | \psi_{jt}, \kappa_{jt}, \kappa_{j,t+1}, a_j, c_j, \rho_j) &\propto p(\psi_{jt} | \lambda_{jt}, a_j, c_j, \rho_j) p(\kappa_{j,t+1} | \lambda_{jt}, a_j, c_j, \rho_j) p(\lambda_{jt} | \kappa_{jt}, a_j, c_j, \rho_j) \\ &\propto \lambda_{jt}^{c_j} e^{-\frac{\lambda_{jt}}{\psi_{jt}}} \lambda_{jt}^{\kappa_{j,t+1}} e^{-\frac{a_j}{c_j} \frac{\rho_j}{1-\rho_j} \lambda_{jt}} \lambda_{jt}^{a_j + \kappa_{jt} - 1} e^{-\frac{a_j}{c_j} \frac{1}{1-\rho_j} \lambda_{jt}} \\ &= \lambda_{jt}^{a_j + c_j + \kappa_{jt} + \kappa_{j,t+1} - 1} e^{-\lambda_{jt} \left( \frac{a_j}{c_j} \frac{1+\rho_j}{1-\rho_j} + \frac{1}{\psi_{jt}} \right)}, \end{aligned}$$

which is the kernel of a  $\mathcal{G} \left( a_j + c_j + \kappa_{jt} + \kappa_{j,t+1}, \frac{a_j}{c_j} \frac{1+\rho_j}{1-\rho_j} + \frac{1}{\psi_{jt}} \right)$  distribution. Modifications are needed for  $t = 0$  and  $t = T$ . For  $t = 0$ , note that:

$$\begin{aligned} p(\lambda_{j0} | \kappa_{j1}, a_j, c_j, \rho_j) &\propto p(\kappa_{j1} | \lambda_{j0}, a_j, c_j, \rho_j) p(\lambda_{j0} | a_j, c_j) \\ &\propto \lambda_{j0}^{\kappa_{j1}} e^{-\frac{a_j}{c_j} \frac{\rho_j}{1-\rho_j} \lambda_{j0}} \lambda_{j0}^{a_j - 1} e^{-\frac{a_j}{c_j} \lambda_{j0}} \\ &= \lambda_{j0}^{a_j + \kappa_{j1} - 1} e^{-\frac{a_j}{c_j} \frac{1}{1-\rho_j} \lambda_{j0}}, \end{aligned}$$

which is the kernel of a  $\mathcal{G}\left(a_j + \kappa_{j1}, \frac{a_j}{c_j} \frac{1}{1-\rho_j}\right)$  distribution. For  $t = T$ , note that

$$\begin{aligned} p(\lambda_{jT}|\psi_{jT}, \kappa_{jT}, a_j, c_j, \rho_j) &\propto p(\psi_{jT}|\lambda_{jT}, c_j)p(\lambda_{jT}|\kappa_{jT}, a_j, c_j, \rho_j) \\ &\propto \lambda_{jT}^{c_j} e^{-\frac{\lambda_{jT}}{\psi_{jT}}} \lambda_{jT}^{a_j+\kappa_{jT}-1} e^{-\frac{a_j}{c_j} \frac{1}{1-\rho_j} \lambda_{jT}} \\ &= \lambda_{jT}^{a_j+c_j+\kappa_{jT}-1} e^{-\lambda_{jT} \left(\frac{a_j}{c_j} \frac{1}{1-\rho_j} + \frac{1}{\psi_{jT}}\right)}, \end{aligned}$$

which is the kernel of a  $\lambda_{jT}|\psi_{jT}, \kappa_{jT}, a_j, c_j, \rho_j \sim \mathcal{G}\left(a_j + c_j + \kappa_{jT}, \frac{a_j}{c_j} \frac{1}{1-\rho_j} + \frac{1}{\psi_{jT}}\right)$  distribution.

Finally, in step (c)(4)  $\psi_{jt}|\lambda_{jt}, w_{jt}, c_j$  follows an inverse Gamma distribution, as

$$\begin{aligned} p(\psi_{jt}|w_{jt}, \lambda_{jt}, c_j) &\propto p(w_{jt}|\theta_j, \psi_{jt})p(\psi_{jt}|\lambda_{jt}, c_j) \\ &\propto \psi_{jt}^{-\frac{1}{2}} e^{-\frac{w_{jt}^2}{2\theta_j\psi_{jt}}} \psi_{jt}^{-c_j-1} e^{-\frac{\lambda_{jt}}{\psi_{jt}}} \\ &= \psi_{jt}^{-(c_j+\frac{1}{2})-1} e^{-\frac{1}{\psi_{jt}} \left(\lambda_{jt} + \frac{w_{jt}^2}{2\theta_j}\right)} \end{aligned}$$

which is the kernel of an  $\psi_{jt}|w_{jt}, \lambda_{jt}, c_j \sim \mathcal{G}^{-1}\left(c_j + \frac{1}{2}, \lambda_{jt} + \frac{w_{jt}^2}{2\theta_j}\right)$  distribution.

### D.2.1 Efficient sampling of $\kappa_{jt}$

To sample  $\kappa_{jt}$  in step (c)(2) in Algorithm 1, we need to sample from a  $(d \times T)$ -dimensional discrete random variable, where  $P_{jt,k} = \Pr(\kappa_{jt} = k|\kappa_{j,s}, \psi_{j,r}, \rho_j, a_j, c_j)$ , for  $s \in \{\max(t-1, 1), \min(t+1, T)\}$  and  $r \in \{\max(t-1, 1), t\}$ , is given by the unnormalized weights provided in (58), divided by the normalization constant given in (59).

To this end, we can exploit that  $P_{jt,k}$  satisfies a recursive scheme. The initial value  $P_{jt,0}$  is given by:

$$P_{jt,0} = \frac{1}{{}_2F_1(a_{jt}^\kappa, b_{jt}^\kappa; c_j^\kappa; z_{jt}^\psi)},$$

with successive values for  $k \geq 1$  given by,

$$P_{jt,k} = P_{jt,k-1} \phi_{jt,k}, \quad \phi_{jt,k} = \frac{(a_{jt}^\kappa + k - 1)(b_{jt}^\kappa + k - 1) z_{jt}^\psi}{(c_j^\kappa + k - 1) k}. \quad (60)$$

This makes it possible to sample the entire  $(d \times T)$ -dimensional discrete random variable  $\boldsymbol{\kappa} = \{\{\kappa_{jt}\}_{j=1}^d\}_{t=1}^T$  with a recursive algorithm that does not require precomputation of  $P_{jt,k}$  for all  $k = 0, \dots, K_{\max}$ :

- (a) Sample a  $(d \times T)$ -array  $\mathbf{U}$  of uniform random numbers and determine the  $(d \times T)$ -array  $\mathbf{P}^{(0)}$  of initial probabilities  $P_{jt,0}$ . If  $\mathbf{U}_{jt} \leq \mathbf{P}_{jt}^{(0)}$ , then  $\kappa_{jt} = 0$ .
- (b) Further calculations are only required for the elements in  $\boldsymbol{\kappa}$  where  $\mathbf{U}_{jt} > \mathbf{P}_{jt}^{(0)}$ . For these elements,  $\kappa_{jt}$  is at least equal to 1. We determine  $\mathbf{P}^{(1)}$  from  $\mathbf{P}^{(0)}$  using (60). If  $\mathbf{U}_{jt} < \mathbf{P}_{jt}^{(0)} + \mathbf{P}_{jt}^{(1)}$ , then  $\kappa_{jt} = 1$ .

- (c) Further calculations are only required for the elements in  $\kappa$  where  $\mathbf{U}_{jt} > \mathbf{P}_{jt}^{(0)} + \mathbf{P}_{jt}^{(1)}$ . For these elements,  $\kappa_{jt}$  is at least equal to 2.

This leads to following recursion: starting with  $\kappa^{(0)} = \mathbf{O}$ ,  $\mathbf{U}^{(0)} = \mathbf{U}$ ,  $\mathbf{P}^{(0)}$  and  $k = 0$ , repeat the following steps:

- (a) Increase  $k$  by 1.
- (b) Update  $\kappa^{(k)} = \kappa^{(k-1)} + \mathbb{I}\{\mathbf{U}^{(k-1)} > \mathbf{P}^{(k-1)}\}$ , where the indicator function is applied element-wise.
- (c) Update  $\mathbf{U}^{(k)} = \mathbf{U}^{(k-1)} - \mathbf{P}^{(k-1)}$ .
- (d) Update  $\mathbf{P}^{(k)} = \mathbf{P}^{(k-1)} \odot \mathbf{\Phi}^{(k)}$ , where the elements  $\phi_{jt,k}$  of the  $(d \times T)$  matrix  $\mathbf{\Phi}^{(k)}$  are given in (60) and  $\odot$  is element-wise matrix multiplication.
- (e) Terminate the recursion if  $\mathbf{U}^{(k)} < \mathbf{P}^{(k)}$  for all elements or  $k > K_{\max}$ .

Ticker	Name	Reg. office	Ticker	Name	Reg. office
ADS.DE	Adidas	Germany	IBE.MC	Iberdrola	Spain
ADYEN.AS	Adyen	Netherlands	ITX.MC	Inditex	Spain
AD.AS	Ahold Delhaize	Netherlands	IFX.DE	Infineon Technologies	Germany
AI.PA	Air Liquide	France	INGA.AS	ING Group	Netherlands
AIR.PA	Airbus	France	ISP.MI	Intesa Sanpaolo	Italy
ALV.DE	Allianz	Germany	KER.PA	Kering	France
ABI.BR	Anheuser-Busch InBev	Belgium	KNEBV.HE	Kone	Finland
ASML.AS	ASML Holding	Netherlands	OR.PA	L'Oréal	France
CS.PA	AXA	France	LIN.DE	Linde plc	Ireland
BAS.DE	BASF	Germany	MC.PA	LVMH	France
BAYN.DE	Bayer	Germany	MBG.DE	Mercedes-Benz Group	Germany
BBVA.MC	BBVA	Spain	MUV2.DE	Munich Re	Germany
SAN.MC	Banco Santander	Spain	RI.PA	Pernod Ricard	France
BMW.DE	BMW	Germany	PHIA.AS	Philips	Netherlands
BNP.PA	BNP Paribas	France	PRX.AS	Prosus	Netherlands
CRG.IR	CRH	Ireland	SAF.PA	Safran	France
BN.PA	Danone	France	SAN.PA	Sanofi	France
DB1.DE	Deutsche Börse	Germany	SAP.DE	SAP	Germany
DPW.DE	Deutsche Post	Germany	SU.PA	Schneider Electric	France
DTE.DE	Deutsche Telekom	Germany	SIE.DE	Siemens	Germany
ENEL.MI	Enel	Italy	STLA.MI	Stellantis	Netherlands
ENI.MI	Eni	Italy	TTE.PA	TotalEnergies	France
EL.PA	EssilorLuxottica	France	DG.PA	Vinci SA	France
FLTR.IR	Flutter Entertainment	Ireland	VOW.DE	Volkswagen Group	Germany
RMS.PA	Hermès	France	VNA.DE	Vonovia	Germany

Table 2: Tickers, names and registered offices of companies that comprise the EURO STOXX 50 index. Companies shaded red were excluded from the application in Section 4 due to data availability issues.

## Appendix E Data overview

Table 2 gives an overview of the companies that comprise the EURO STOXX 50 index. Importantly, the tickers (e.g. FLTR.IR) used in the plots in Section 4 are connected to the company names, as the connection between the two is often non-obvious. The companies shaded in red were excluded from the application, either due to the number of missing values or because the data on the returns did not reach back far enough.